Subcortically generated movements activate motor cortex during sleep and wake in rats through postnatal day 24

Madilyn R. Reid[1]*, Nicholas J. Sattler[1]*, and James C. Dooley[1,2†‡]

[1]Department of Biological Sciences, Purdue University, West Lafayette, Indiana
[2]Purdue Institute for Integrative Neuroscience,
Purdue University, West Lafayette, Indiana

*These authors contributed equally.
†Corresponding author: James C. Dooley, Ph.D. (jcdooley@purdue.edu)
‡Lead Contact: James C. Dooley

Keywords: Primary motor cortex, development, sensorimotor, REM sleep, myoclonic twitching, red nucleus, rat

Abbreviated title: Movement-related activity in developing M1

Number of pages: 33

Number of figures: 9, plus 4 supplementary figures

Number of words (abstract): 238

Number of words (introduction): 650

Number of words (discussion): 1362

Conflict of interest statement: The authors declare no competing interests.

Acknowledgments: We thank Mark Blumberg and Greta Sokoloff feedback on earlier versions of this manuscript. This research was supported by the Sleep Research Society Foundation's Career Development Award to J.C.D.

Author contributions: J.C.D. designed research; J.C.D. performed research; M.R.R., N.J.S., and J.C.D. data curation; M.R.R., N.J.S., and J.C.D. analyzed data; M.R.R., N.J.S., and J.C.D. visualization; J.C.D writing – original draft; M.R.R., N.J.S., and J.C.D. writing – review & editing; J.C.D. supervision; J.C.D. resources

Abstract

During early postnatal life, cortical motor control emerges from complex interactions between cortical and subcortical circuits. Although activity-dependent processes are essential for primary motor cortex (M1) to develop motor functions, the precise activity patterns that precede this transition remain unclear. To track the development of movement-related activity in M1, we recorded single-unit activity in the forelimb region of M1 in unanesthetized, head-fixed rats across sleep and wake at postnatal days (P) 12, 16, 20, and 24. At every age, a subset of M1 neurons showed somatotopically precise responses to spontaneous limb twitches that occur during REM sleep, along with strong responses to wake movements. From P12 to P24, the proportion of M1 neurons that showed twitch-related activity decreased, twitch-related activity became more temporally refined, and a larger fraction of spikes occurred before movement onset. To compare M1's developmentally nascent activity with that of an established motor structure, we performed simultaneous recordings in M1 and the red nucleus (RN) at P24. Compared to M1, more RN activity preceded twitches and wake movements. Further, RN activity was more diverse, with neurons firing during specific wake movements, whereas wake-movement-related activity in M1 was largely non-selective. These results suggest that through P24, movement-related activity in M1 reflects predicted and actual sensory feedback across both sleep and wake, whereas movement-related activity in RN drives limb movements across both sleep and wake. Altogether, these data highlight the continued importance of subcortically generated movements in shaping M1's functional organization.

Significance Statement

In adults, primary motor cortex (M1) is widely recognized for its role in initiating voluntary movements and guiding motor learning. However, during early development, our findings show that M1 processes activity related to self-generated limb movements but does not drive the production of those movements. Using simultaneous recordings from M1 and the red nucleus (RN) of developing rats, we show that although M1 shows movement-related activity during wake and sleep, RN remains the principal driver of behavior through at least postnatal day 24. These results refine our understanding of early movement-related activity and highlight the possibility that both sleep-related twitches and wake movements shape sensorimotor development by driving neural activity in M1 and RN.

Introduction

In placental mammals, primary motor cortex (M1) is viewed as the key player in motor production and learning (see Peters et al., 2017). However, it is increasingly clear that motor control necessitates coordinated activity from the entire brain, including the thalamus, basal ganglia, cerebellum, and brainstem (Kawai et al., 2015; Sauerbrei et al., 2020; Ruder et al., 2021; Inagaki et al., 2022; Lopez-Virgen et al., 2023; Yang et al., 2023). The contributions of these subcortical structures are impossible to ignore in infancy, as M1 is not yet capable of driving movement (Martin, 2005; Young et al., 2012;

Williams and Martin, 2015; Singleton et al., 2021). Instead, in numerous mammals, including rats, anatomical and functional evidence shows that limb movements are generated by brainstem motor nuclei, with the red nucleus (RN) of the midbrain playing a critical role throughout this period (Ulfig and Chan, 2001; Rio-Bermudez et al., 2015; Williams and Martin, 2015).

But the developing M1 is not silent, instead responding to sensory feedback from movements produced during periods of REM sleep (Dooley and Blumberg, 2018; Glanz et al., 2021; Gómez et al., 2021). This behavioral state specificity is because prior to postnatal day 10 (P10), the sensory feedback resulting from wake movements is actively inhibited (Tiriac et al., 2014; Tiriac and Blumberg, 2016). As a result, M1 is particularly responsive to the myoclonic twitches produced during REM sleep. This state-dependent sensory activity is not unique to M1, as similar inhibition of sensory feedback during wake movements has been observed in primary somatosensory and visual cortex at these ages (Mukherjee et al., 2017; Murata and Colonnese, 2018; Dooley et al., 2020). Consequently, throughout the first ten postnatal days, most sensorimotor activity is driven by twitches, which ultimately produces the required circuitry for M1 motor control (Chakrabarty and Martin, 2005; Dooley and Blumberg, 2018; Dooley et al., 2020).

As development progresses, M1 gradually assumes its role in motor control, which in rats begins to emerge around P25 and is adult-like around P60 (Young et al., 2012; Singleton et al., 2021). Chronic inhibition of M1 across early development impedes the development of cortical motor control but also alters the maturation of subcortical motor structures like RN (Williams et al., 2014; Williams and Martin, 2015), suggesting that the development of cortical motor control is highly dependent on neural activity (Chakrabarty and Martin, 2005; Yang and Martin, 2023). However, little is known about the patterning of movement-related neural activity in M1 prior to the onset of cortical motor control, nor how this movement-related activity compares to activity of established motor structures like RN.

Here, we perform extracellular recordings in the forelimb representation of M1 in unanesthetized rats spanning P12 to P24 as they cycle between non-REM (NREM) sleep, REM sleep, and wake. This developmental window includes the refinement of thalamic inputs to M1 and the developmental emergence of cerebellar-dependent internal models (Dooley et al., 2021). By analyzing movement-related activity during both sleep and wake, we show that neurons in M1 respond to REM-sleep associated twitches and wake movements at all ages (P12 to P24). Taking advantage of the somatotopic discreteness of twitches, we show that neurons in the forelimb region of M1 respond exclusively to forelimb movements at all ages. Thus, sensory responses in M1 are somatotopically refined by P12. However, even at P24, movement-related activity in M1 does not systematically precede twitches or wake movements, suggesting that M1 is not yet involved in generating movement. To compare M1 neural activity with an established motor structure, we performed simultaneous extracellular neural recordings in M1 and RN of P24 rats. We found that activity in RN precedes twitches and wake movements, while activity in M1 lags behind activity in RN. Further, we found a subset of neurons in RN fire during specific limb movements, whereas neurons in M1 fire more indiscriminately. Altogether, our data suggests that through P24, forelimb movements are predominantly generated by RN.

Materials and Methods

Code Accessibility

All original code has been deposited at https://github.com/jcdooley/XXX and is publicly available as of the date of publication. Any additional information required to reanalyze the data reported in this paper is available from the corresponding author upon request.

Experimental model and subject details

For the first experiment, neurophysiological recordings of M1 were obtained from Sprague-Dawley Norway rats (*Rattus norvegicus*) at P12 (N = 9 pups; 30.8 ± 2.4 g; 3 male), P15-16 (hereafter P16; N = 12 pups; 43.7 ± 3.0 g; 8 male), P18-P20 (hereafter P20; N = 12 pups; 56.1 ± 4.4 g; 7 male), and P22-P24 (hereafter P24; N = 8 pups; 68.5 ± 4.7 g; 6 male). Animals within the same age group were always from different litters. Although the focus here is on M1 activity, recordings were performed in the forelimb region of M1 and either the ventral lateral or the ventral posterior nucleus of thalamus. The thalamic data has been published and described previously (Dooley et al., 2021). For the second experiment, dual neurophysiological recordings were performed in M1 and the RN at P24 (N = 7 pups, 65.8 ± 5.2 g; 3 male). To be included in the analysis, animals needed more than 40 right forelimb twitches and at least one neuron had to be responsive to right forelimb twitches. This criterion led to the exclusion of 2 animals.

Pups were born and raised in standard laboratory cages (48 × 20 × 26 cm) in a temperature- and humidity-controlled room on a 12:12 light-dark cycle, with food and water available ad libitum. The day of birth was considered P0 and litters were culled to eight pups by P3. All pups had at least four littermates until P12 and at least two littermates on the day that neurophysiological recordings were performed. No pups were weaned before testing. All experiments were conducted in accordance with the National Institutes of Health (NIH) Guide for the Care and Use of Laboratory Animals (NIH Publication No. 80–23) and were approved by the Institutional Animal Care and Use Committees at the University of Iowa and Purdue University.

Method Details

Surgery. As described previously (Dooley et al., 2021), a pup with a healthy body weight and (for P12 pups) a visible milk band was removed from the litter and anesthetized with isoflurane gas (3–5%; Phoenix Pharmaceuticals, Burlingame, CA). The hair on the top of the head was shaved and care was taken to ensure that the vibrissae were intact. For sleep/wake state determination, two custom-made bipolar hook electrodes (0.002-inch diameter, epoxy coated; California Fine Wire, Grover Beach, CA) were inserted into the nuchal and biceps muscles contralateral to the neural recordings. Carprofen (5 mg/kg SC; Putney, Portland, ME) was administered as an anti-inflammatory analgesic.

The skin above the skull was carefully removed and an analgesic (bupivicane; Pfizer, New York, NY) was applied topically to the skull. The skull was then dried with bleach. For P20 and P24 rats, any bleeding around the skull was cauterized to ensure that it was completely dry prior to the application of a headplate. Vetbond (3M, Minneapolis, MN) was then applied to the skin surrounding the incision, and a custom-manufactured head-plate (Neurotar, Helsinki, Finland) was secured to the skull using cyanoacrylate adhesive.

A trephine drill (1.8 mm; Fine Science Tools, Foster City, CA) was used to drill a hole into the skull above the forelimb representation of M1 (0.5 mm anterior and 2.2–2.5 mm lateral to bregma). When thalamic recordings were also performed (as reported in Dooley et al., 2021), a second hole was drilled above thalamus (2.0–2.8 mm caudal to bregma, 2.2–2.5 mm lateral to the sagittal suture). In Experiment 2, when RN recordings were performed, a second hole was drilled above RN (5.2 mm caudal to bregma, 0.4 to 0.8 mm lateral to the sagittal suture). A small amount of peanut oil was applied to the dura to prevent desiccation of the underlying tissue. This surgical procedure lasted approximately 30 min.

While recovering from anesthesia, the pup was secured to a custom-made head-fixation plate secured to a Mobile HomeCage (NTR000289-01; Neurotar). The height of the pup's head off the floor was adjusted depending on its age so that, when the pup was exhibiting atonia during REM sleep, its body rested on its elbows (P12: 35 mm; P16: 38 mm; P20 and P24: 40 mm). Electromyography (EMG) wires were carefully secured behind the pup's back to ensure that they would not get tangled. Pups recovered from anesthesia within 15 minutes and were acclimated to the head-fix apparatus for 1 to 2.5 hours. This period of acclimation allowed the recording electrodes to stabilize and the return of normal spiking activity (Domínguez et al., 2021). When recording began, all pups were exhibiting typical behavioral and electrophysiological features of sleep and wake (i.e., twitching, grooming, locomotion).

Recording Environment. Electrophysiological recordings were performed in a Faraday cage illuminated by flicker-free red LEDs (630 nm; Waveform Lighting, Vancouver, WA). Continuous white noise (70 dB) was present throughout the recording session. To maximize REM sleep, the room's temperature was maintained between 26.5 and 29° C (Szymusiak and Satinoff, 1981). The animal's head was positioned away from the entry to the room so that it could not see the experimenter entering or leaving, which was infrequent. For the comfort of both the experimenter and the subject, the experimenter was outside the room and monitoring the animal and data acquisition remotely.

Electrophysiological Recordings. The nuchal and biceps EMG electrodes were connected to the analogue inputs of a Lab Rat LR-10 acquisition system (Tucker Davis Technologies, Gainesville, FL). The EMG signals were sampled at approximately 1.5 kHz and high-pass filtered at 300 Hz.

Before insertion, we coated a 16-channel silicon depth electrode (A1x16-3mm-100-177-A16) with fluorescent DiI (Vybrant DiI Cell-Labeling Solution; Life Technologies, Grand Island, NY). Electrodes were inserted using a multiprobe manipulator (New Scale Technologies; Victor, NY) controlled by an Xbox controller (Microsoft, Redmond, WA). The electrode was inserted into cortex until all electrode sites were beneath the dura (approximately 1500 μm). A chlorinated Ag/Ag-Cl wire (0.25 mm diameter; Medwire, Mt.

Vernon, NY) inserted into occipital cortex contralateral to the cortical recording sites served as both reference and ground. Neural signals were sampled at approximately 25 kHz. A high-pass filter (0.1 Hz) and a harmonic notch filter (60, 120, and 180 Hz) were applied.

Electrophysiological data were acquired continuously for 3-6 h using SynapseLite (Tucker Davis Technologies). The Mobile HomeCage enabled stable head-fixation throughout the recording session while rats could freely locomote, groom, and sleep.

Video Collection and Synchronization. As described previously (Dooley et al., 2020), video data were synchronized to electrophysiological recordings so that we could quantify movements and behavioral state. Rats were surrounded by a clear enclosure within the Mobile HomeCage, enabling unimpeded visual access. The video was recorded using a single Blackfly-S camera (FLIR Integrated Systems; Wilsonville, Oregon) positioned at a 45° angle (relative to the pup's head) and centered on the right forelimb, contralateral to the M1 recordings. This angle provided an unobstructed view of the right whiskers, forelimb, hindlimb, and tail. Video was collected in SpinView (FLIR Integrated Systems) at 100 frames/s, with a 7 ms exposure time and 720- x 540-pixel resolution.

Video frames were synchronized to the electrophysiological record using an external time-locking stimulus. A red LED, controlled by SynapseLite (Tucker Davis Technologies), was in view of the camera and pulsed every 3 s for a duration of 100 ms. Custom MATLAB scripts determined the number of frames between each LED pulse to check for dropped frames. Although infrequent, when the number of frames between pulses was not equal to 300 (3 s inter-pulse interval x 100 frames/s), a "dummy frame" was inserted in that location. This ensured that the video and electrophysiological data were synchronized to within one frame (10 ms) throughout data collection.

Histology. At the end of the recording session, the pup was euthanized with ketamine/xylazine (10:1; >0.08 mg/kg) and perfused with 0.1 M phosphate-buffered saline (PBS) followed by 4% paraformaldehyde (PFA). The brain was extracted and post-fixed in 4% PFA for at least 24 h and was then transferred to a 30% sucrose solution at least 24 h before sectioning.

To confirm the electrode's location in M1, the neocortex was either flattened and sectioned tangentially to the pial surface or sectioned coronally. When sectioned tangentially, the right cortical hemisphere was dissected from the subcortical tissue and flattened between two glass slides (separated using a 1.5 mm spacer) for 5-15 min. Small weights (10 g) applied light pressure to the upper slide. Regardless of the plane of section, the tissue was sectioned at 80 µm. Wet-mounted sections were imaged at 2.5x using a fluorescent microscope and digital camera (Leica Microsystems, Buffalo Grove, IL) to identify the location of the DiI.

Cortical sections were stained for cytochrome oxidase (CO), which reliably delineates primary sensory areas in cortex at these ages (Seelke et al., 2012). Briefly, cytochrome C (3 mg per 10 mL solution; Sigma-Aldrich), catalase (2 mg per 10 mL solution; Sigma-Aldrich) and 3,3'-diaminobenzidine tetrahydrochloride (DAB; 5 mg per 10 mL solution; Spectrum, Henderson, NV) were dissolved in a 1:1 dilution of PB-H2O and distilled water. Sections were developed in well plates on a shaker at 35–40°C at approximately 100

rotations per min for 3–6 h, after which they were washed in PBS, mounted onto glass slides, and allowed at least 48 h to dry. Once dry, sections were placed in citrus clearing solvent (Richard-Allan Scientific) and cover slipped.

RN sections were stained using cresyl violet, which reliably delineates the large cell bodies in RN from the surrounding tissue (Rio-Bermudez et al., 2015). On mounted gelatin-coated slides, sections were dehydrated via submersion in increasing concentrations of ethanol in distilled water for 5-min each. Sections were then defatted using two 5-min washes of citrus clearing solution (Richard-Allan Scientific), followed by a rinse in 100% ethanol. Sections were then stained in a 0.1% cresyl violet solution for 5-10 min, rinsed in distilled water, and immersed in a differentiation solution (70% ethanol with 0.1-0.5% acetic acid) until cell nuclei were maximally differentiated. Finally, sections were fully dehydrated in 100% ethanol for 5-min, followed by 5-min in 2 subsequent rinses of citrus clearing solvent, and cover slipped.

Stained sections were imaged at 2.5x or 5x magnification. Multiple images were combined into a single composite image (Microsoft Image Composite Editor; Microsoft, Redmond, WA) and the electrode location were visualized in relation to areal, nuclear, and laminar boundaries of the stained tissue. M1 recordings were included in subsequent analyses when they were between 0 and 1.2 mm medial to the forelimb representation of S1. RN recordings were included in subsequent analyses when the electrode track went through the large cell bodies of RN.

Local Field Potential. For all local field potential (LFP) analyses, the raw neural signal was down sampled to ~1000 Hz and smoothed using a moving Gaussian kernel with a half-width of 0.5 ms.

Classification of Behavioral State. As described previously, behavior, nuchal EMG signals, and cortical LFPs were used to identify periods of wake, REM sleep, and NREM sleep (Dooley et al., 2021). Wake was characterized by periods of high nuchal muscle tone and wake-related behaviors (e.g., locomotion, grooming). REM sleep was characterized by the occurrence of myoclonic twitches against a background of muscle atonia. At P16 and later, REM sleep was also accompanied by the presence of continuous theta oscillations in thalamic and RN recordings. During NREM sleep, we observed high cortical delta power, behavioral quiescence, and moderate nuchal muscle tone, although periods of high delta power were sometime accompanied by nuchal muscle atonia. Periods not assigned as REM or NREM sleep were designated as wake. Active wake was defined as that part of the wake period that was less than 3 s following an ROI-defined period of movement (see below).

Power Spectrum Analysis. LFPs were analyzed by behavioral state (quiet wake, active wake, REM sleep, and NREM sleep). Power spectral densities were calculated from the LFP signal using MATLAB's pspectrum() function with default settings. The resulting raw power spectra were then normalized relative to quiet wake by converting power values to decibels (dB). Quiet wake was chosen as the baseline for normalization because it represents a state with minimal movement-related artifact and lacks prominent state-

specific oscillations (such as theta oscillations characteristic of REM sleep, or delta oscillations and sleep spindles characteristic of NREM sleep).

ROI Movement Classification. As described previously (Dooley et al., 2021), to quantify periods of movement, we used custom MATLAB scripts to detect frame-by-frame changes in pixel intensity within regions-of-interest (ROIs). The number of pixels within the ROI that exhibited an intensity change >5% were summed. This calculation was performed for each frame, resulting in a 100 Hz time series of changes in pixel intensity which was used to identify periods of movement.

For twitches, the movement timeseries for a ROI containing the body part of interest (e.g., forelimb) was visualized alongside the video using Spike2 (Version 8; Cambridge Electronic Design, Cambridge, UK). Peaks in the time series were confirmed to be twitches of the appropriate body part. Twitch onset was defined as the first frame in which movement occurred (using the ROI timeseries data described above). For the forelimb, hindlimb, and tail, this method effectively counted every visible twitch, since even twitches in rapid succession have distinct onset and offset times. However, for whisker twitches, alternating protractions and retractions did not always have clear temporal boundaries, thus making it difficult to determine when one whisker twitch ended, and another began. In these instances, only the first whisker twitch in a series of twitches was counted.

For wake movements, an ROI of the entire animal was used. Multiple wake movements typically occur in quick succession; however, we wanted to be sure that every labeled wake movement identified a transition from no movement to movement. Thus, we often marked only the first wake movement in a bout of wake movements, marking subsequent movements only when they were accompanied by at least 500 ms of behavioral quiescence.

Quantification and statistical Analysis

Spike Sorting. SynapseLite files were converted to binary files using custom MATLAB scripts and sorted with Kilosort 2.0 (Pachitariu et al., 2016). Briefly, data were whitened (covariance-standardized) and band-pass filtered (300-5000 Hz) before spike detection. Template-matching was implemented to sort the event waveforms into clusters. The first-pass spike detection threshold was set to six standard deviations below the mean and the second-pass threshold was set to five standard deviations below the mean. The minimum allowable firing rate was set to 0.01 spikes/s and the bin size for template detection was set to 262,400 sample points, or approximately 11 s. All other Kilosort parameters were left at their default values.

Clusters were visualized and sorted in Phy2 (Rossant and Harris, 2013). Putative single units had spike waveforms that reliably fit within a well-isolated waveform template, appeared in a principal component analysis as a distinct cluster, and had an auto-correlogram with a decreased firing rate at a time lag of 0 (indicative of a unit's refractory period).

Clusters meeting the first two criteria but not the third were considered multi-units and were discarded from analysis. Any putative unit with a waveform template indicative of electrical noise, a firing rate < 0.01 spikes/s, or amplitude drift across the recording period

was discarded. Cross-correlograms of all single- and multi-units on nearby channels were compared. If cross-correlograms and auto-correlograms were similar, clusters were merged and (if appropriate) reclassified as multi-units.

Determination of Twitch- and Wake-Movement-Responsiveness. All analyses of neural data were performed in MATLAB using custom-written scripts. The relation between neural activity and twitches or wake movements was assessed as follows. First, all twitches of each body part (forelimb, hindlimb, whiskers, tail) were behaviorally scored. For each body part that had more than 20 twitches, perievent histograms of neural activity were constructed (window size: -3 to 3 s; bin size: 10 ms). Next, we determined the mean baseline firing rate from -3 to -0.5 s. Finally, we z-scored the perievent histograms by subtracting the baseline from the raw perievent histograms and dividing this value by the standard deviation of the baseline. A neuron was considered “responsive” to twitches if it showed a clear peak with a z-score of at least 3.5 for at least one body part. A neuron was considered “responsive” to wake movements using the same criteria, but with perievent histograms triggered on wake movements. All other neurons were classified as “non-responsive.”

To accurately determine a neuron’s preferred somatotopic response, we only analyzed twitches for a given body part that were separated from twitches of other body parts by at least 100 ms. The preferred body part for each neuron was the body part with the largest peak in the z-scored perievent histogram. At all ages, neurons in the forelimb region of M1 responded to right forelimb twitches, not right hindlimb, tail, or whisker twitches.

ROI-based Movement Analysis. For each movement type (twitches of different body parts and wake movements), we calculated the average displacement produced by that movement for each pup. To ensure subsequent twitches (of the same or different body parts) did not influence the average displacement of a twitch, for this analysis, we used the same subset of twitch triggers used in the somatotopy analysis above (i.e., twitches with inter-twitch-intervals of at least 100 ms). Median average displacement was calculated over all triggered twitches (or wake movements) at each timepoint. Because the size of the ROI used to assess movements varied across age and body part, median values for each animal were always normalized and then averaged.

Movement kinematics. For the M1-RN dataset, a point tracking the centroid position of the palm of the left forelimb and radiocarpal joint of the wrist for the right forelimb was used to quantify movement trajectories using DeepLabCut (Mathis et al., 2018). Manually labeled frames taken across periods of REM sleep and wake adjacent to movement from all animals were used to initially train the network. Frames with poor marker estimates from newly analyzed videos were then additionally labeled and used to re-train the network until mean likelihoods of 0.85 were achieved across previously detected twitches and wake movements. For all videos, 1 mm = 5.75 pixels.

Movement angle and amplitude. Using the previously established movement initiation times, the movement initiation location was defined as the position of the limb on the frame of movement onset. Using this point as the origin, we calculated the amplitude and angle of the limb at every timepoint for 150 ms for twitches, and 500 ms for wake movements. Movement amplitude was then defined as the limb’s peak displacement

within the window, and the movement angle was defined as the limb's angle at peak displacement.

Width at Half-Height. To measure width at half-height, the neural data were first smoothed using a 5-bin kernel and then upscaled from 10 ms bins to 1 ms bins using the interp1() function in MATLAB. The data were then normalized so that the baseline was equal to 0 and the peak was set to 1. The width at half-height (in ms) was calculated as the number of continuous bins greater than 0.5 around the peak of the normalized data.

Proportion of spikes before twitch onset. The proportion of spikes before movement onset was calculated by approximating the integral of z-scored perievent histograms triggered on twitch onset using the trapz() function in MATLAB. First, a window was selected that was inclusive of the period of elevated activity for the neurons being analyzed (-0.2 to 0.75 s for the M1 development analysis, and -0.2 to 0.2 s for the M1-RN analysis). The proportion of activity before twitch onset was calculated by dividing the integral from -0.2 to 0 s by the integral of the entire window. For three neurons, a negative value in the numerator produced a nonsensical negative proportion of spikes preceding twitch onset. Thus, for these neurons the proportion was set to 0.

Coefficient of variation of neural response. The coefficient of variation was calculated from the number of spikes within a window that included twitch- and wake-movement-related neural activity (-70 to 70 ms for twitches; -100 to 500 ms for wake movements). For each neuron, the standard deviation of the spikes was divided by the mean number of spikes within that window.

Statistical Analyses. All statistical tests were performed using MATLAB. Alpha was set at 0.05 for all analyses; when appropriate, the Bonferroni procedure was used to correct for multiple comparisons. Unless otherwise stated, mean data are always reported with their standard error of the mean (SEM). Data were tested for significance using a one-way ANOVA, two-way ANOVA, or t test. Categorical data were tested for significance using a Chi-squared test. Violin plots were constructed absent outliers, which were determined using the isoutlier() function in MATLAB. This function excludes data points that are more than three scaled median-absolute-deviations from the median.

Results

Features of REM and NREM sleep in M1 activity through P24

To establish whether REM sleep twitches continue to drive activity in M1 beyond P12, we recorded single-unit activity in head-fixed, unanesthetized rats at P12, P16, P20, and P24. The recording environment was designed to be permissive of REM sleep. First, rats were tested in the Mobile HomeCage, an air table that allows rats to locomote while head-fixed (**Figure 1A**). Second, we increased the temperature of the recording environment to about 29° C, which promotes REM sleep (Szymusiak and Satinoff, 1981). Together, this allowed us to record significant periods of REM and NREM sleep on the day of surgery. Extracellular activity was recorded in the forelimb region of M1 (P12: N = 9 pups, 121 neurons; P16: N = 12 pups, 177 neurons; P20: N = 12 pups, 172 neurons; P24: N = 8 pups, 87 neurons; **Figure 1C, D**). Neural activity, electromyographic activity of the nuchal and biceps muscles, and high-speed video (100 frames/s) were recorded continuously for 3-6 h, and representative data from each behavioral state and each age can be seen in **Figure 2**. Recordings were performed entirely during the lights-on period (1000 to 1800 hours).

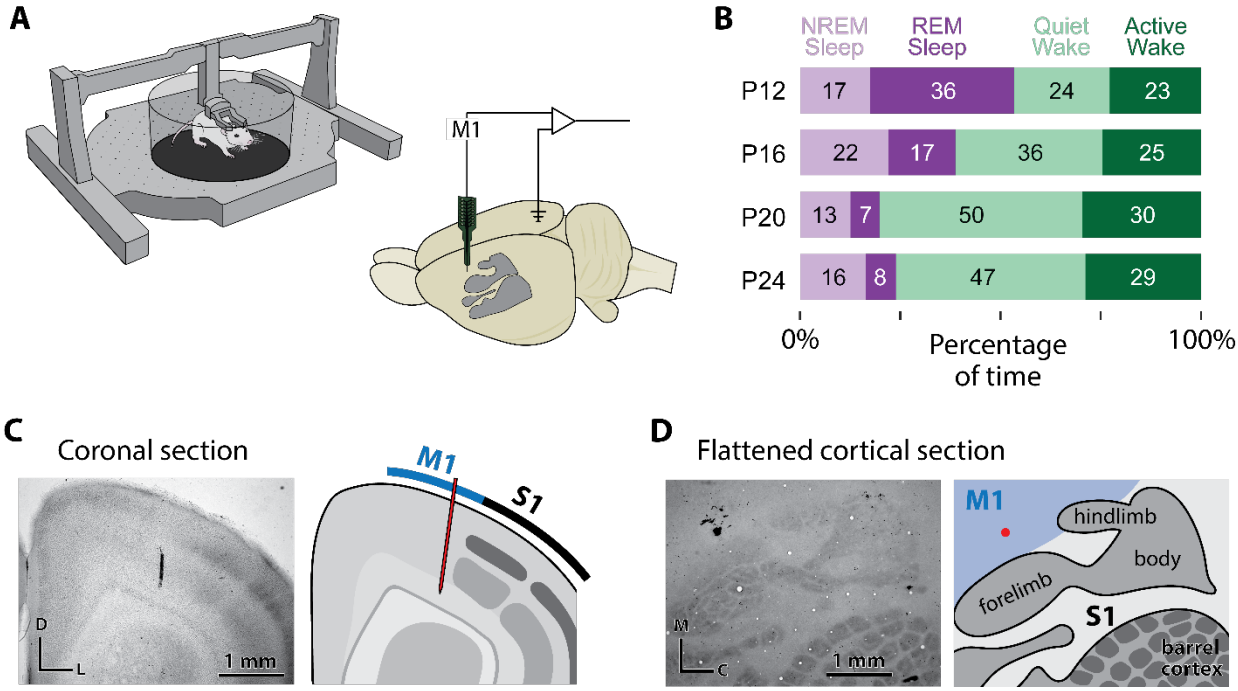

Figure 1. Recording environment, behavioral state quantification, and M1 recording verification
(A) Left: An illustration of the Mobile HomeCage used to record behavioral and electrophysiological data from head-fixed rat pups across sleep and wake. Right: A schematic of the rat brain with the primary somatosensory cortex (S1) shaded in gray, highlighting the approximate recording location in M1 and the reference/ground in the contralateral occipital cortex.
(B) Mean percentage of time spent in NREM sleep (light purple), REM sleep (dark purple), quiet wake (light green), and active wake (dark green) at each age. Numbers in each bar indicate the mean percentage of total recording time for that state across all animals.
(C) Representative coronal section stained for cytochrome oxidase showing the DiI-labeled electrode track in M1. Borders of primary somatosensory cortex are shown in gray; the DiI-labeled track is visible in the forelimb region of M1.
(D) Representative flattened cortical section stained for cytochrome oxidase showing the DiI-labeled electrode track in M1. Conventions as in C.

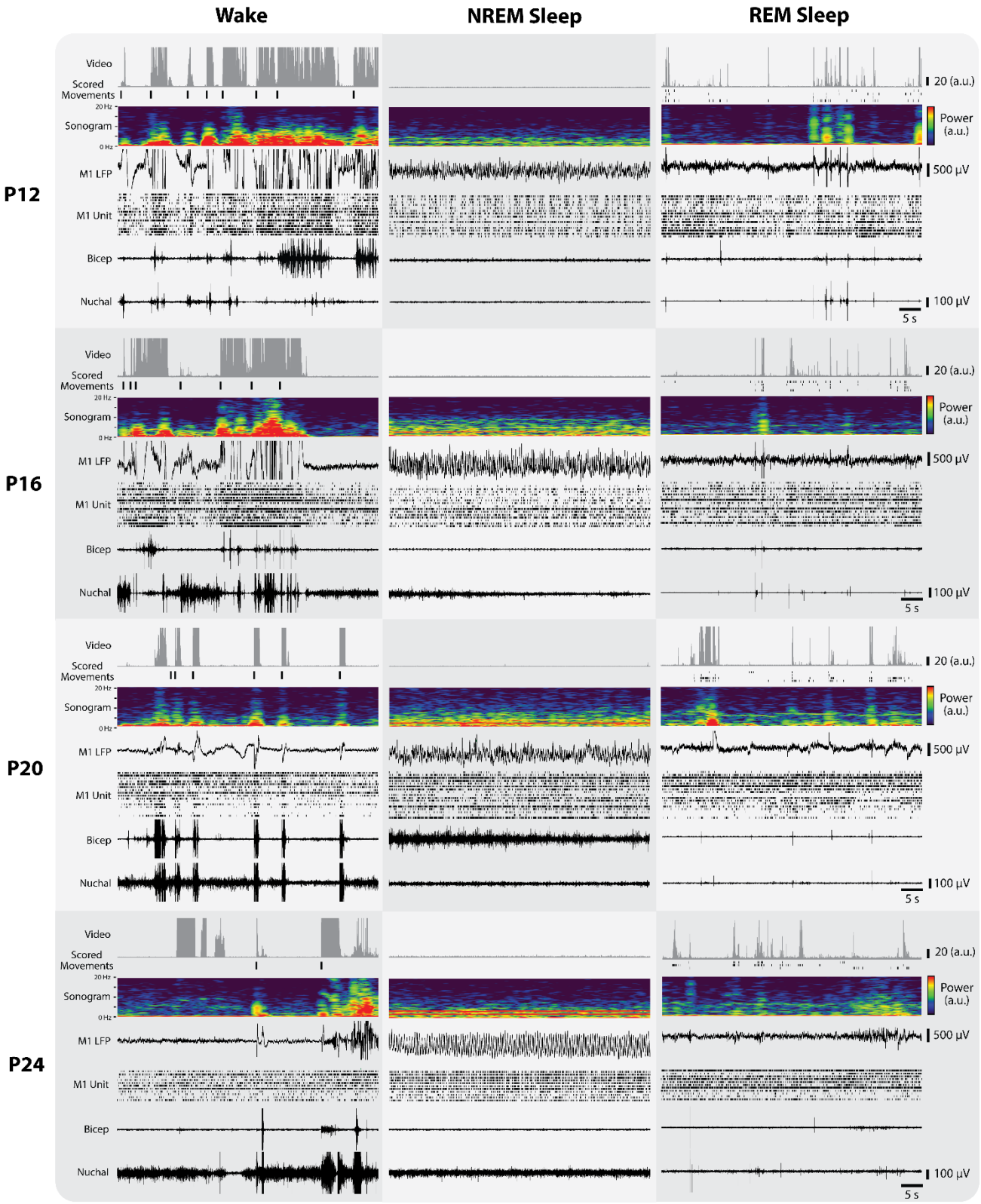

Figure 2. Behavioral and electrophysiological data across wake, NREM sleep, and REM sleep
For each age (P12, P16, P20, P24), a 50-s segment of continuous data is shown for wake, NREM sleep, and REM sleep. **Top to bottom**: ROI-based movement analysis of the entire rat (as detected by pixel-based motion detection), scored movements (wake movements during wake, twitches during REM sleep), M1 LFP, single-unit activity in M1 (each row corresponds to a separate unit), and biceps and nuchal EMG signals. Rows of scored twitches are forelimb, hindlimb, whisker, and tail, from top to bottom. These representative examples demonstrate distinct patterns of behavioral, neural, and muscular activity at each developmental age.

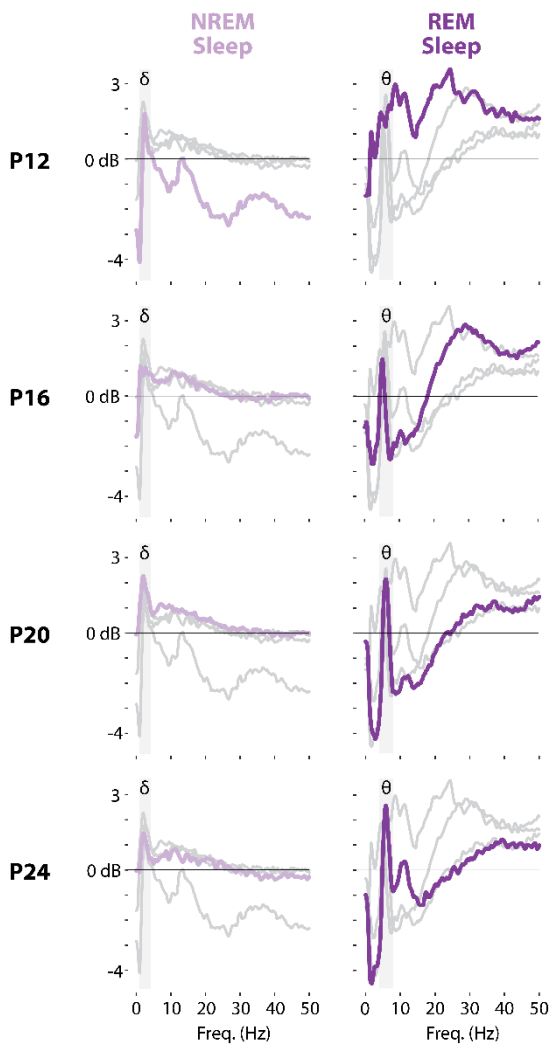

Figure 3. Developmental changes in oscillatory power during NREM and REM sleep
Normalized power spectra (1–50 Hz) at each age (P12, P16, P20, P24) are plotted relative to quiet wake. **(Left)** NREM sleep (light purple) exhibits a pronounced delta peak at all ages. **(Right)** REM sleep (dark purple) demonstrates an emerging theta peak from P16 onward. For each panel, data for the focal age are highlighted in color, whereas spectra for the other three ages are shown in gray for comparison. These findings illustrate the marked developmental changes in delta and theta oscillations across sleep states.

All rats cycled between NREM sleep, REM sleep, and wake throughout the recording sessions. As expected, the percentage of time spent in REM sleep decreased across age, whereas the percentage of time spent in quiet wake increased (see **Figure 1B**). Consistent with prior work, NREM sleep was associated with increased delta power (1-4 Hz) relative to quiet wake at all ages tested (**Figure 3 left**; Seelke and Blumberg, 2008). At P16, P20, and P24, NREM sleep in M1 also showed an increase in alpha (8-15 Hz) power, likely reflecting the developmental emergence of sleep spindles, which first appear postnatally in humans (Robert, 1982 p.198; Sokoloff et al., 2021). REM sleep showed a markedly different oscillatory profile. Relative to periods of quiet wake, REM sleep in P12 pups was associated with a general increase in power across all frequencies. In P16, P20, and P24 pups, periods of REM sleep showed an increase in theta (4-8 Hz) power, and a decrease in delta and alpha bands, as well as an increase in slow gamma (**Figure 3 right**). The developmental emergence of theta power in M1 between P12 and P16 was also evident in the raw power spectrum; increased power in the theta band was not present at P12, but was present at P16, P20, and P24 (**Figure S1**).

We observed a change in the rate of M1 activity by age during wake ($F_{(3, 553)} = 6.51$; $p < 0.0005$), NREM sleep ($F_{(3, 433)} = 8.2$; $p < 0.0001$), and REM sleep ($F_{(3, 553)} = 3.56$; $p < 0.05$; **Figure S2A-C**). Directly comparing neural activity during wake and REM sleep, we observed more activity during REM sleep than wake at P12 ($t_{120} = 9.278$, $p < 0.0001$), P16 ($t_{176} = 6.55$, $p < 0.0001$), and P20 ($t_{171} = 8.23$, $p < 0.0001$), but not at P24 ($t_{86} = 1.20$, $p = 0.23$; **Figure S2D**). The disappearance of this state-dependent difference in activity at P24 may be why previous studies in adult rodents have not reported more activity during REM sleep compared to wake, as it suggests that the increase in cortical activity during REM sleep is developmentally transient.

Temporal refinement of twitch-related activity from P12 to P24

Over half of M1 neurons responded to forelimb movements during wake and/or forelimb twitches during REM sleep (P12: 77%; P16: 74%; P20: 55%, P24: 65%; **Figure 4A**). At P12, a greater proportion of M1 neurons responded to twitches than wake movements. However, at P16 and beyond, more M1 neurons responded to wake movements than twitches, and only a small minority of neurons that were twitch responsive were not wake responsive (**Figure 4B**). This is not surprising, as wake movements are much longer in duration than twitches, and unlike twitches, involve the simultaneous activation of numerous muscles. Still, at all ages examined, over a quarter of movement-responsive neurons in M1 responded to twitches. Representative twitch responsive neurons at each age can be seen in **Figure 4C**.

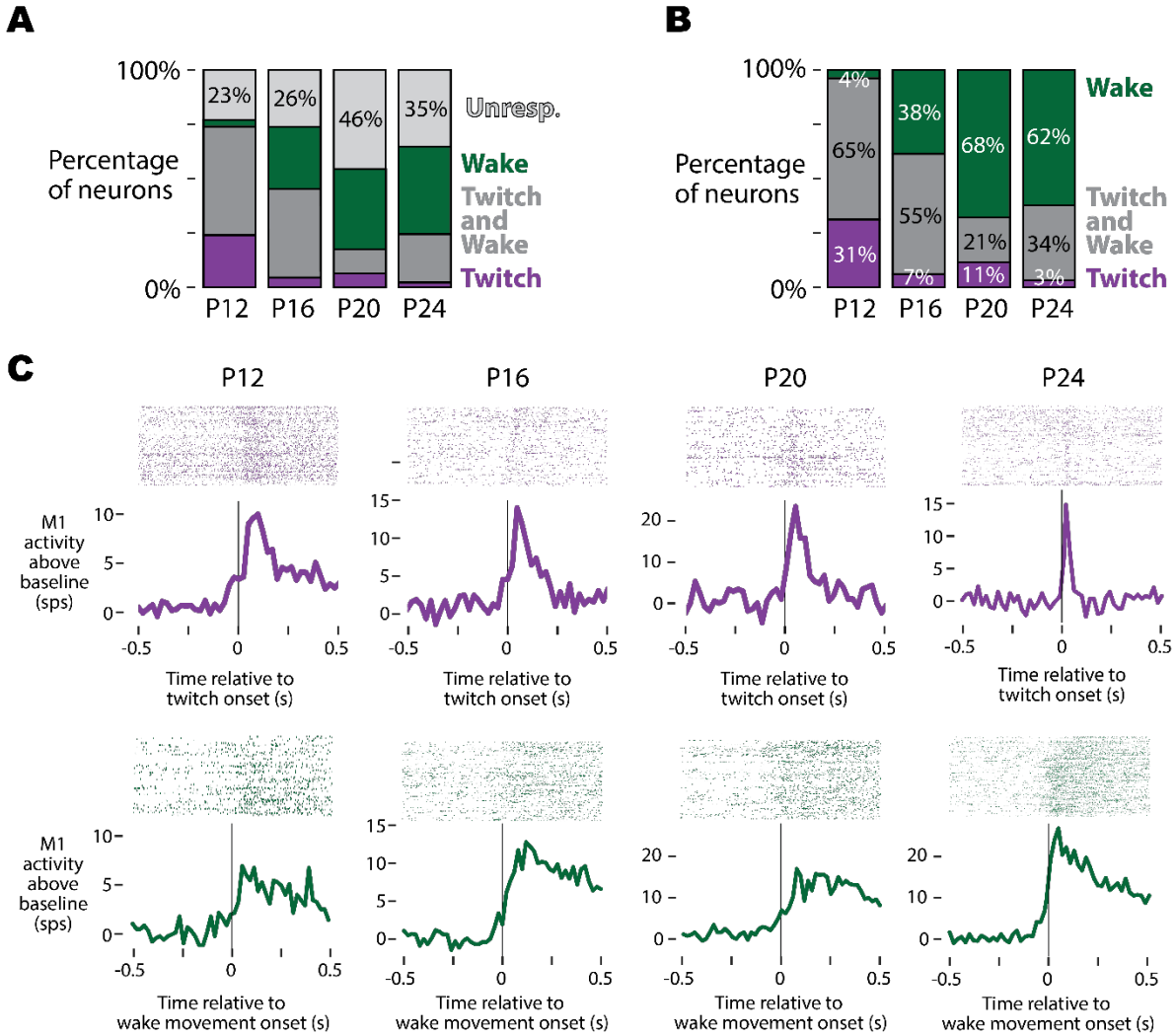

Figure 4. Movement responsiveness in M1 neurons across development
(A) Stacked bar plots showing the percentage of M1 neurons at each age (P12, P16, P20, P24) that respond to self-generated movements (i.e., twitches during REM sleep or wake movements during wake).
(B) Of the movement-responsive neurons identified in (A), the percentage that respond to twitches (purple), wake movements (green), or both (gray) are shown in stacked bars for each age.
(C) Representative M1 neurons from each age (P12, P16, P20, P24), illustrating raster plots (top) and perievent histograms (bottom) triggered on twitch onset (purple) or wake movement onset (green). Each histogram depicts firing rate changes relative to baseline, demonstrating strong but developmentally evolving movement-related activity in M1.

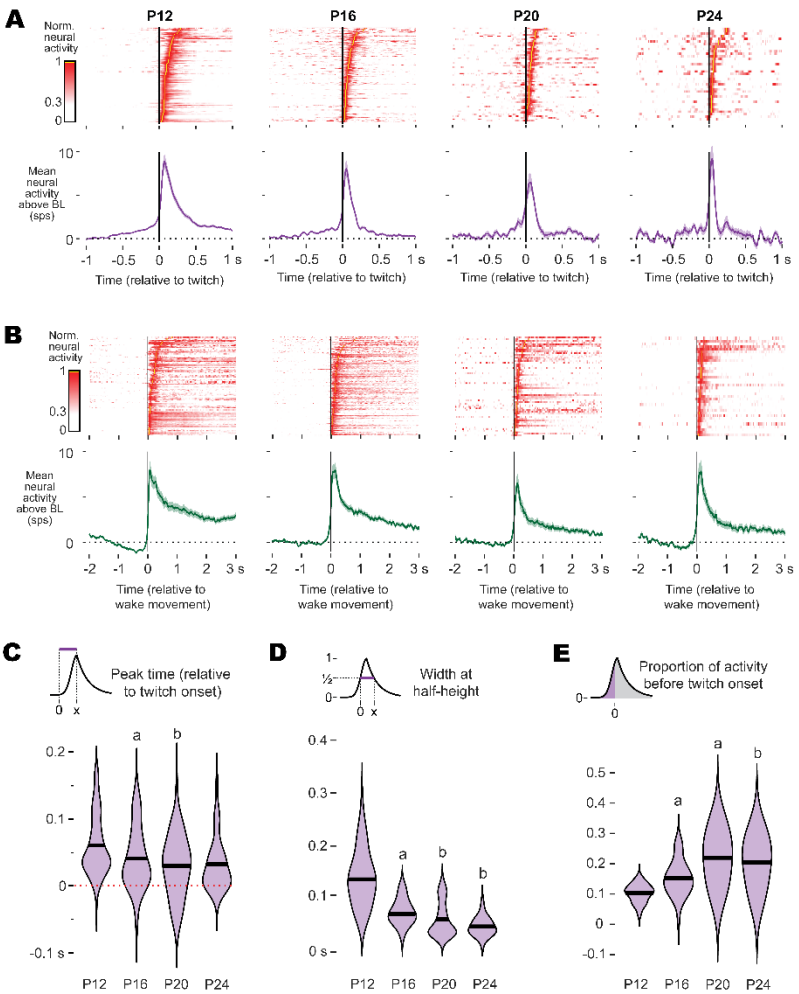

Figure 5. Temporal refinement of twitch- and wake-related M1 activity with age

(A) Top: Heatmaps showing twitch-triggered responses of all twitch-responsive M1 neurons across P12, P16, P20, and P24. Each row corresponds to a single neuron, and color intensity indicates firing rate. Bottom: Mean (±SEM) perievent histograms of these neurons for each age.

(B) Same as (A), but for wake-triggered responses of M1 neurons.

(C) Violin plots of the peak response time (relative to twitch onset) for twitch-responsive M1 neurons by age. The black line represents the mean of the distribution. 'a' indicates a significant difference from the preceding age, whereas 'b' indicates a significant difference from two ages prior.

(D) Same as (C), but for the width at half-height of twitch-triggered responses.

(E) Same as (C), but for the proportion of twitch-related activity that precedes movement. Collectively C-E reveals progressive temporal sharpening of M1 responses to twitches over the course of development.

At a population level, although movement-responsive neurons did show some variability, twitch- and wake-movement-related activity was quite similar within an age (**Figure 5A, B**). However, twitch-responsive neurons in M1 showed temporal refinement across age, mirroring a similar finding in sensory and motor thalamus at these ages (Dooley et al., 2021). As evidence of this refinement, the time of the peak response varied significantly with age ($F_{(3, 305)} = 7.28$; $p < 0.0001$); older animals showed earlier peak activity than younger animals (**Figure 5C**), such that at P20 and P24, the timing of peak M1 responses more closely resembled the timing observed in the ventral lateral nucleus ("motor" thalamus) than the ventral posterior nucleus of the thalamus (see Dooley et al., 2021). In addition, the width at half-height of twitch-responsive neurons also varied significantly with age ($F_{(3, 209)} = 60.4$; $p < 0.0001$), with older ages generally showing briefer responses to twitches compared to younger ages (**Figure 5D**). We next calculated the proportion of twitch-related activity that occurred before twitch onset across ages (**Figure 5E**). This proportion increased significantly with age ($F_{(3, 216)} = 30.5$; $p < 0.0001$), from a mean proportion of 0.10 at P12 to a mean proportion of 0.22 and 0.20 at P20 and P24, respectively. Thus, by P20, about 20% of activity in M1 precedes movement onset.

Twitches are discrete movements, often involving only a single muscle at a time. Because of this, we were able to use these movements to examine whether M1 shows somatotopic precision at these ages. We scored twitches of the right forelimb, right hindlimb, whiskers, and tail. This enabled us to trigger M1 neural activity on temporally-isolated twitches of all 4 of these body parts (i.e. forelimb twitches that do not occur alongside twitches of the hindlimb, whiskers, or tail). All M1 recordings were the region of M1 that shows forelimb movement-related activity in adults (the caudal forelimb area). Our data show that, at all ages examined (P12 to P24), twitch-responsive neurons in the forelimb region of M1 only respond to forelimb twitches (**Figure S3**). This suggests that at least course somatotopy is present in M1 by P12.

Altogether, these results suggest that M1's role in motor production through P24 remains limited. This is consistent with previous reports using intracortical microstimulation (ICMS) to assess M1 motor output (Young et al., 2012; Singleton et al., 2021). However, we did observe an increase in the proportion of twitch-related activity that precedes movement across these ages (see **Figure 5E**), suggesting that by P24, activity in M1 may be beginning to resemble movement-related activity seen in a traditional motor structure. To better contextualize this transition, we next compared activity in M1 of P24 rats with activity in RN, the midbrain motor nucleus believed to be responsible for movements, including twitches, throughout infancy (Williams et al., 2014; Rio-Bermudez et al., 2015).

RN activity precedes twitches and wake movements at P24

Prior work demonstrates that RN generates forelimb twitches through at least P12 (Rio-Bermudez et al., 2015), and work on M1 and RN interactions suggests that RN's role in motor control persists through the developmental emergence of M1 motor control (Williams et al., 2014; Williams and Martin, 2015). Thus, RN is presumed to be responsible for forelimb twitches through P24, although this has yet to be demonstrated. To investigate RN's role in movement production and to compare the activity of M1 to a known motor structure, we performed dual recordings in M1 and RN of P24 rats (**Figure 6A, B**; N = 7 animals; 112 Neurons in M1; 111 Neurons in RN). In RN, baseline firing rates significantly differed across REM sleep and wake ($t_{110} = 8.86$, $p < 0.0001$) with RN firing nearly twice as much during REM sleep ($\bar{x} = 13.1$ spikes/s) than during wake ($\bar{x} = 7.2$ spikes/s; **Figure 6C**).

A majority of RN neurons from P24 rats showed an increase in activity during forelimb movements (60%; **Figure 6D**). 61% of the forelimb-responsive neurons showed twitch related activity, whereas 85% showed wake-movement related activity (**Figure 6D**).

A representative RN neuron showing twitch and wake-movement related activity is shown in **Figure 6E**. Movement-related activity in RN was much more heterogeneous than was seen previously in M1, particularly with respect to wake movements. For example, whereas some twitch-responsive RN neurons showed movement-related activity for nearly every wake movement (see **Figure 6E, right**), other twitch-responsive RN neurons showed no activity—or even inhibition—during wake movements (**Figure 6F**).

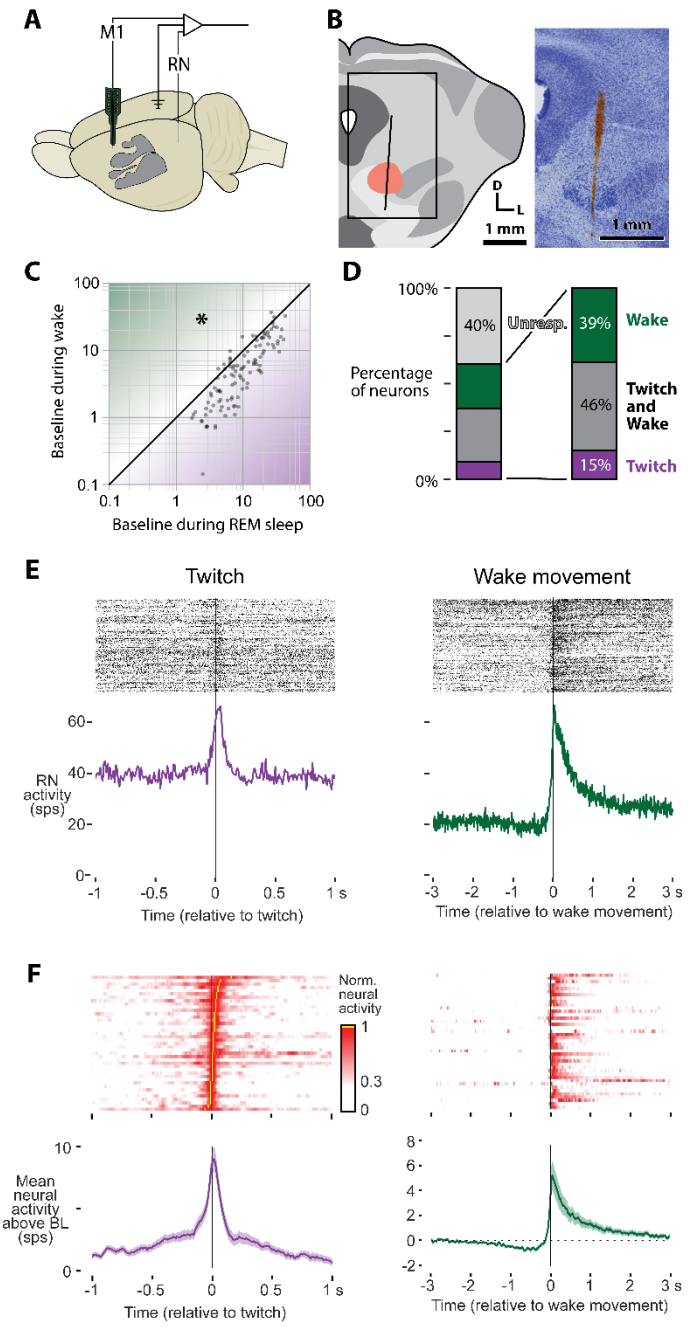

Figure 6. RN recordings and responsiveness to movement at P24
(A) Schematic of the rat brain illustrating the dual recording sites in M1 and RN in P24 rats.
(B) Cartoon representation of a coronal section through the midbrain, showing the RN (red oval) and a representative electrode track for RN recordings. The rectangle on the left indicates the region enlarged on the right, which depicts the Nissl-stained section with the electrode track (red) passing through RN.
(C) Scatter plot of baseline RN neuronal activity during REM sleep (x-axis) versus wake (y-axis). Most RN units exhibit higher firing rates in REM sleep than in wake, and this difference is significant (asterisk).
(D) Stacked bar plots showing the proportion of RN neurons responsive to forelimb movements. The subplots on the right illustrate the fraction of those responsive neurons that react to twitches (purple), wake movements (green), or both (gray). This parallels the format of Figures 4A and 4B for M1.
(E) Representative RN neuron with raster plots (top) and averaged perievent histograms (bottom) for twitch- (left, purple) and wake-movement-triggered (right, green) responses.
(F) Heatmaps of all twitch-responsive RN neurons (top) and mean (±SEM; bottom) triggered on twitch onset (left) and wake movement onset (right), akin to Figures 5A and 5B for M1.

Movement-related activity in M1 lags RN at P24

The population-level activity seen in this second cohort of M1 recordings from P24 rats (**Figure 7A, B**) closely resembles those reported earlier (see **Figures 4, 5**). In aggregate, movement-related activity in M1 and RN is similar, with both structures showing brief increases in neural activity around twitches and longer duration increases in neural activity around wake movements (**Figure 7B, D top**). However, in RN, twitch-related activity increases earlier than in M1, a difference that is particularly apparent when subtracting normalized twitch-related activity of responsive RN neurons from equivalent M1 neurons (**Figure 7B bottom**). This difference between twitch-related activity in M1

and RN can be exhibited quantitively: In RN, twitch-related activity peaks nearly 20 ms earlier than M1 (15 ms and 34 ms, respectively; t_{98} = -5.18, $p < 0.0001$; **Figure 7E**). Because of more preceding activity, twitch-related activity in RN is also broader than in M1 (t_{102} = -4.18, $p < 0.0001$; **Figure 7F**), and a greater proportion of activity in RN preceded twitch onset compared to M1 (0.45 and 0.29, respectively; **Figure 7G**; t_{109} = -8.35, $p < 0.0001$).

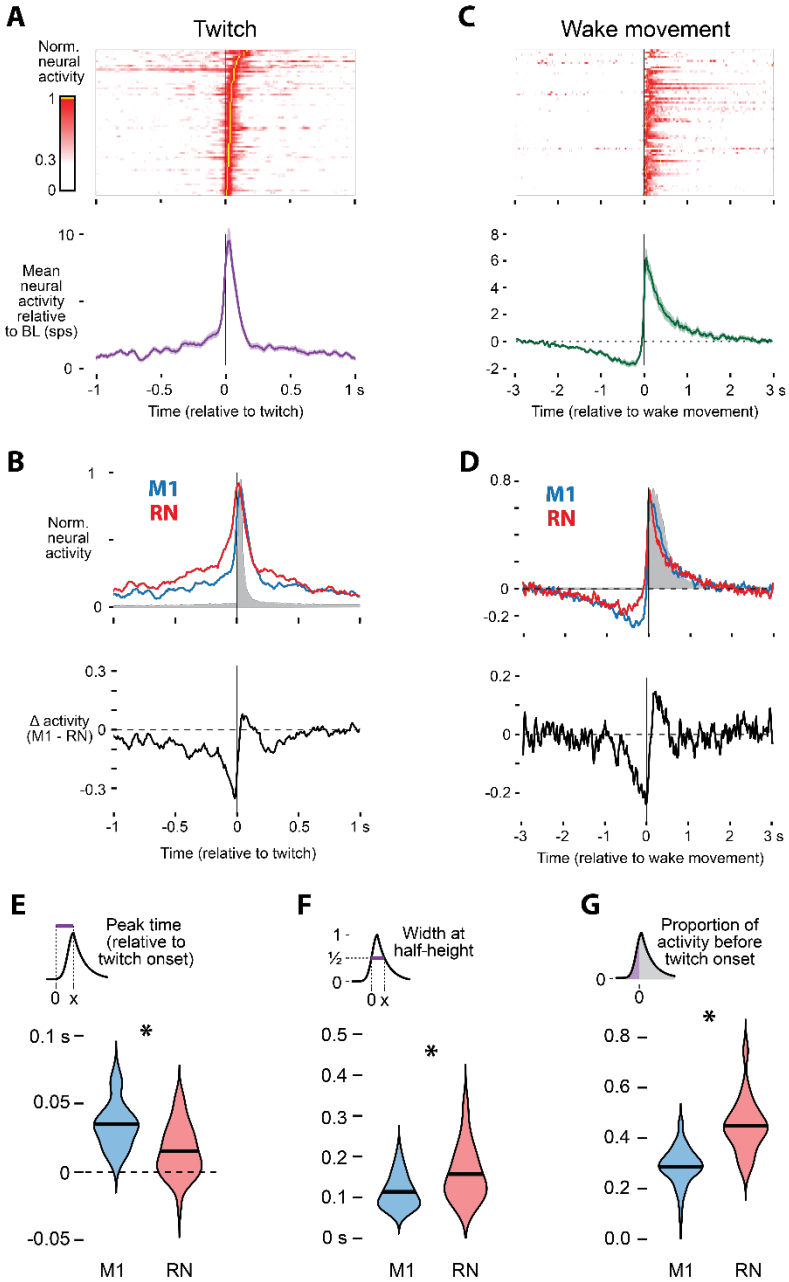

Figure 7. Comparison of twitch- and wake-related activity between M1 and RN at P24
(A) Heatmap of twitch-related responses of all twitch-responsive M1 neurons recorded during dual M1–RN recordings (compare to Figure 6F for RN).
(B) Top: Averaged, normalized twitch-triggered firing rates of M1 (blue) and RN (red) neurons. The gray shaded region indicates median displacement from the twitch. Bottom: The difference in normalized firing rates (M1 minus RN) shows RN activity precedes M1 activity.
(C) Same as A, but for wake movements.
(D) Same as B, but for wake movements.
(E) Violin plots of peak twitch-related activity for twitch-responsive M1 (blue) and RN (red) neurons, showing that RN responses peak significantly earlier than those in M1. Asterisk signifies a significant difference between groups.
(F) Violin plots of the width at half-height for neurons that show twitch-related activity. Conventions as in E.
(G) Violin plots of the proportion of activity that precedes twitch onset for neurons that show twitch-related activity. Conventions as in E.

Altogether, we found that RN shows considerably more activity preceding movement onset compared to M1, strongly suggesting RN remains the principal driver of forelimb twitches through P24. Similarly, aggregate wake-movement-related activity in RN also precedes that in M1 (**Figure 7D, bottom**), supporting the idea that RN continues to drive wake movements at these ages. However, unlike twitches, wake movements unfold over

several hundred milliseconds, resulting in sustained neural activity that spans the entirety of the movement. Because of this extended duration, the proportion of neural activity occurring before wake movement onset appears relatively small compared to twitches, as illustrated by the difference in timescales in **Figures 7C** and **7D**. Additionally, our method of defining wake movement onset—requiring approximately 500 ms of behavioral quiescence—creates uncertainty in determining an appropriate baseline activity level, as the period immediately before wake movements is the only time we can be certain the animal is quiescent. Because we measured baseline activity as the average activity 0.5 to 3 s before movement onset, our baseline estimate is inflated by activity from preceding wake movements. Thus, the apparent decrease in neural activity below baseline prior to wake movements reflects contamination by earlier movements, rather than suppression of activity (see **Figures 6F** and **7C, D**).

In adult animals, RN neurons are known to produce specific wake movements, including behaviors like locomotion (Rho et al., 1999). If RN is similarly responsible for producing wake movements in P24 rats, we reasoned that individual RN neurons might also display firing patterns selective to specific wake behaviors. Thus, to investigate whether neurons in RN and M1 fire selectively during distinct types of wake movements, we next quantified limb kinematics for both twitches and wake movements and related these measures with neural activity recorded simultaneously from each structure.

Wake-movement-related activity is more variable in RN than M1

Wake-movement-related activity in RN can differ sharply from movement to movement. We often observed individual neurons in RN showing increased activity for some wake movements and suppression for others (**Figure 8A**). This makes sense given the diverse kinematics of wake behaviors, which are highly variable (**Figure 8B**). Across all 7 animals, we found that wake movement responses showed significantly higher response variability in RN than in M1, as indicated by a higher coefficient of variation in RN ($t_{211} = -4.93$, $p < 0.0001$; **Figure 8C**). Previous studies in adults demonstrate that electrically stimulating specific locations in M1 and RN trigger specific movements (Rho et al., 1999; Küchler et al., 2002; Halley et al., 2020). Wake behaviors are highly diverse—ranging from locomotion to grooming to reaching—yet each neuron is thought to drive only one of these actions; therefore, an individual neuron should fire exclusively when the animal performs that neuron's specific movement.

To examine whether neural response variability tracks movement variability, we applied DeepLabCut to trace right- and left-forelimb trajectories (**Figure S4A, B**). Taking the neuron in **Figure 8A**, we sorted each wake movement by the number of RN spikes within a 300 ms response window: events with more than 50% less activity (2 or fewer spikes) were classified as "non-preferred," whereas those with 50% more activity (6 or more spikes) were classified as "preferred" (**Figure 8D**). This yielded two sharply contrasting perievent histograms (**Figure 8E, G**). Strikingly, the "preferred" wake movements isolated

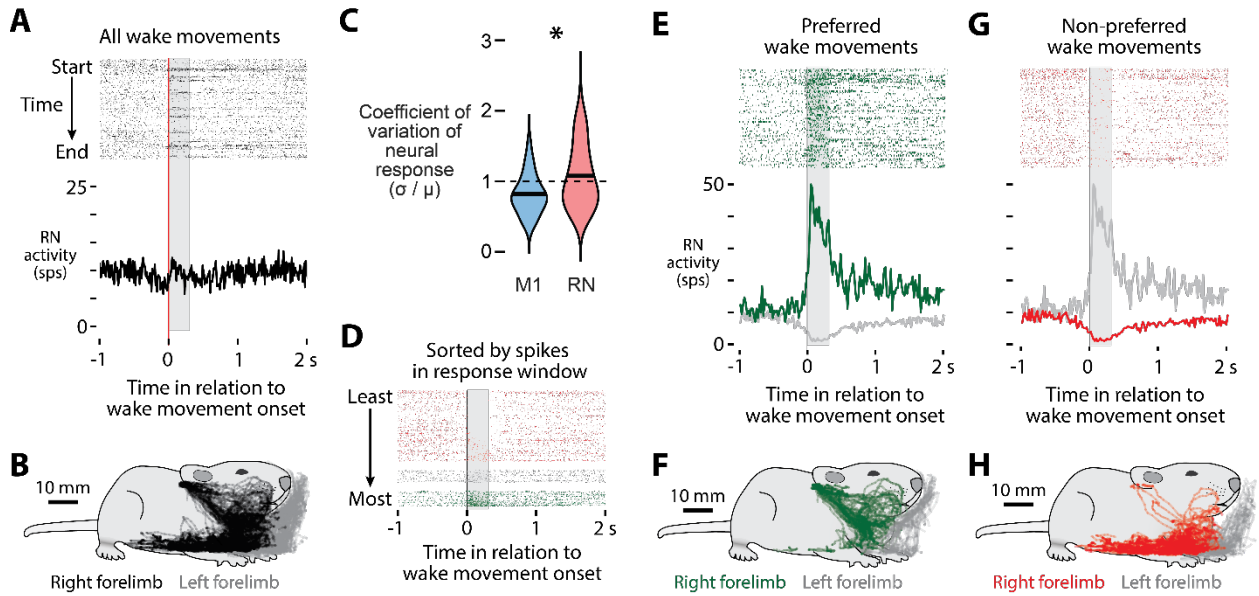

Figure 8. Activity related to wake movements is highly variable in RN
(A) Raster and perievent histogram for all wake movements of a representative RN neuron that responds to only a subset of wake movements.
(B) Location of the right and left forelimbs (black and grey, respectively) for all triggered wake movements.
(C) Violin plots of the coefficient of variation of neural responses to wake movements for all M1 and RN neurons. Wake movement activity in RN is more variable than M1.
(D) The raster plot shown in **A**, sorted by the number of spikes in the response window.
(E) Raster and perievent histogram for the preferred wake movements.
(F) Location of the right and left forelimbs (green and grey, respectively) for wake movements accompanied by a neural response.
(G) Same as in **E**, but for the wake movements that did not produce a neural response.
(H) Same as in **F**, but for the wake movements that did not produce a neural response.

the right forelimb movements to the pup's right ear and vibrissae (**Figure 8F**), and video review confirmed that these movements were overwhelmingly bilateral ($\chi^2 = 37.9$, N = 454, $p < 0.001$), occurring during bouts of facial grooming. In contrast, the "non-preferred" category comprised the rest of the wake repertoire, including postural adjustments and locomotion (**Figure 8H**).

Thus, wake-movement-related activity in the RN is not always uniform; the same neuron can switch from excitation to inhibition depending on the movement being produced. Similar mixed responses have been documented in M1 of adult rodents through targeted stimulation (Peters et al., 2017), hinting that distinct movement categories may differentially recruit these circuits. Motivated by this, we undertook a fine-grained kinematic assessment of forelimb behaviors to compare whether RN and M1 encode specific wake movements.

RN neurons are more movement-selective than M1 neurons

To examine whether all neurons in M1 and RN responded to specific forelimb movements, or more generally to all forelimb movements, we used the limb position data to perform a kinematic analysis of twitches and wake movements. We then related this kinematic

analysis to neural activity, on a movement-by-movement basis. Not surprisingly, wake movements were much larger in amplitude than twitches, with wake movements averaging 6.95 mm and twitches averaging 0.96 mm (**Figure S4C**). The amplitude and angle of all wake movements and twitches can be seen in **Figures S4D and E**, respectively (N = 4365 wake movements, N = 3766 twitches; pooled across 7 animals). A majority of right forelimb movements were forwards or backwards from a resting position (0° and 180°), which during wake consists largely of locomotion and postural control movements. Because the pup's limbs are resting on the surface of the Mobile HomeCage, very few movements were in the downward direction (270°), however a subset of movements were in the upwards direction, (90°) towards the face. Video analysis confirmed that these movements contained the overwhelming majority of facial grooming.

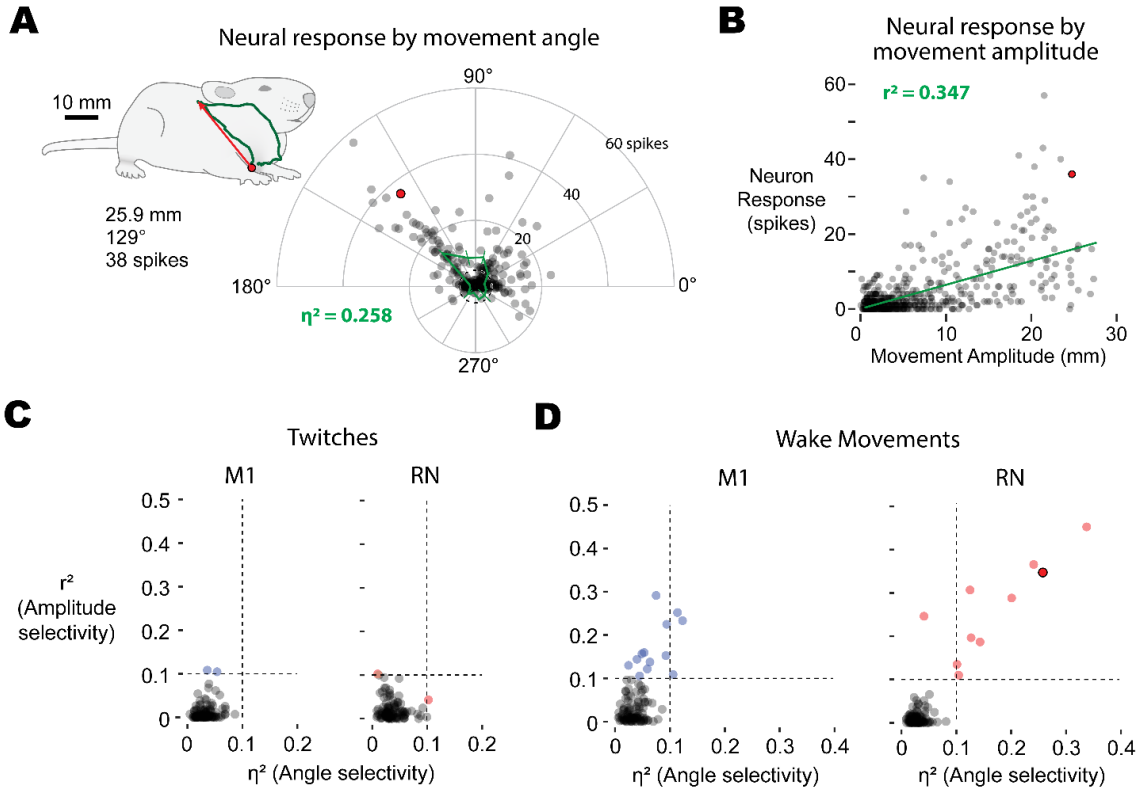

Figure 9. RN neurons exhibit greater movement selectivity than M1 neurons
(A) Polar plot for a representative RN neuron showing spike counts as a function of wake-movement direction (12 bins). The inset traces one example movement: the right forelimb starts at the red circle and reaches a maximum displacement of 25.9 mm at 129° (red arrow); this movement is highlighted with a red dot here and in B. Direction accounts for 25.8 % of the neuron's response variance ($\eta^2 = 0.258$).
(B) The same neuron's firing versus movement amplitude; green line, linear fit ($r^2 = 0.347$).
(C) For twitches, neither movement angle (η^2) nor amplitude (r^2) explains much response variance in M1 (left) or RN (right); only two neurons in each region exceed the 0.1 threshold (dashed lines).
(D) For wake movements, a larger subset of M1 neurons shows amplitude selectivity (elevated r^2), whereas RN neurons more often exhibit combined angle- and amplitude-tuning (both η^2 and $r^2 > 0.1$). The red-outlined point marks the example neuron from **A**–**B**.

After determining twitch and wake movement trajectories, we next established whether movement direction and movement amplitude explain variability of M1 or RN neural responses. For each neuron, we quantified the number of spikes within the "response window" of each movement (-70 to 70 ms for twitches, and -100 to 500 ms for wake movements). We then calculated how much of the response variability is explained by movement amplitude or movement direction (quantified by grouping movements in 12 equally sized directional bins; see **Figures S4D, E** and **9A**).

The response variability explained by movement angle and movement amplitude of the neuron in **Figure 8** are shown in **Figures 9A** and **9B**, respectively. A single representative grooming movement (**Figure 9A inset**) is illustrated with the red dot, while all other wake movements are illustrated with a gray dot. This neuron showed a strong response to movements towards the face and ears (60° to 150°) and a weaker than average response to movements in other directions, such that movement direction explained 25.8% of neural response variability. Likewise, movement amplitude was positively correlated with neural response, explaining 34.7% of response variability. For this neuron, twitch-related activity did not meaningfully explain response variability, with movement direction and amplitude explaining 4.5% and 0.1% of response variability, respectively (data not shown).

Across the population, limb kinematics did not predict twitch-evoked firing in either M1 or RN (**Figure 9C**). However, wake movements revealed a subtle yet critical distinction between these regions. Although only a minority of neurons were kinematically tuned (13 of 112 neurons in M1, 10 of 111 neurons in RN), the nature of this tuning differed markedly. In RN, nearly every kinematically selective neuron (9 of 10; see **Figure 9D**) showed selectivity for both amplitude and direction, clearly encoding specific movement trajectories. In contrast, kinematically selective M1 neurons were only amplitude-selective (10 of 13). And although three neurons surpassed the threshold for direction selectivity, their direction tuning was relatively weak, barely exceeding our threshold ($\eta^2 \approx 0.1$). Thus, the clear and robust coupling of amplitude and direction selectivity observed in RN contrasts sharply with M1's predominantly amplitude-based selectivity, reinforcing the conclusion that RN's neurons more directly encode motor commands, whereas M1's neurons are largely reflective of generalized sensory feedback.

Discussion

By performing extracellular neurophysiology in M1 from P12 and P24 (**Figure 1**), we demonstrate that adult-like oscillatory patterns during wake, NREM sleep, and REM sleep emerge as early as P20 (**Figures 2, 3,** and **S1**). Further, throughout this developmental window, M1 encodes self-generated movements—both REM-sleep twitches and a wide range of wake movements—yet does not appear to initiate them (**Figures 4** and **5**). Exploiting the discreteness of twitches, we found that by P12 M1 is already somatotopically organized (**Figure S3**) and that its twitch-related responses become progressively faster and sharper across age (**Figure 5C-E**). Simultaneous recordings, however, reveal a clear functional split between cortex and brainstem: in P24 pups, neurons in RN not only fire earlier than M1 for both twitches and wake movements (**Figures 6** and **7**) but also display far stronger tuning to the direction and amplitude of individual wake movements (**Figures 8** and **9**). Thus, while M1 is refining its sensory representation of movement, RN activity is consistent with its role as the principal driver of limb behaviors, with individual RN neurons firing selectively during specific wake movements. These results fill a key gap in our understanding of how early sensorimotor activity is patterned, emphasizing that, up through weaning, M1 still depends primarily on reafferent input, rather than producing its own motor commands.

The same movements drive different patterns of M1 activity across development

Although infant M1 is not yet producing movement, it is not silent. M1 undergoes several functional transformations prior to assuming its adult role in behavioral production. From near birth through P10, activity in M1 is heavily patterned by twitches, whereas wake-movement-related activity is inhibited, mirroring the broader sensorimotor system's early reliance on reafferent signals from twitches (Khazipov et al., 2004; Tiriac et al., 2014; Tiriac and Blumberg, 2016). From P10 to P12, functional activity in M1 undergoes several changes. The first change is stopping the inhibition of wake-movement-related activity; a transition that also occurs in the developing somatosensory and visual cortices (Dooley and Blumberg, 2018; Murata and Colonnese, 2018). The second change is in the types of somatosensory inputs that M1 receives. Prior to P12, M1 receives both tactile and proprioceptive inputs from thalamus, in parallel with somatosensory cortex. From P12 onward, M1 only receives proprioceptive inputs from thalamus, becoming reliant on somatosensory cortex for tactile information (Gómez et al., 2021). Finally, population-level activity in M1 goes from bursty to continuous while neurons rapidly decorrelate their sensory responses (Glanz et al., 2021). From the present investigation, we also now know that by P12, M1 shows somatotopic refinement, with the forelimb region of M1 only responding to forelimb twitches (see **Figure S3**).

The present investigation focused on movement-related activity in M1 following the P12 transformation. Prior work on somatosensory and motor thalamus (the ventral posterior and ventral lateral nuclei, respectively) identified P12 to P20 as a period of temporal refinement of movement-related activity (Dooley et al., 2021). Because motor thalamus is the primary thalamic input to M1, it is not surprising that we observed similar temporal

refinement in M1 across this developmental window. In addition, by P20, activity in motor thalamus no longer reflects sensory inputs, but instead reflects a cerebellar-dependent internal model of movement. In the present investigation, the mean latency to peak twitch-related activity in M1 at P20 and P24 is 30 ms (see **Figure 5C**)—the same as previously reported in motor thalamus and equivalent to the peak displacement from twitches. Thus, by P20, movement-related activity in M1 has likely undergone another transformation, representing a cerebellar-dependent internal model of movement.

Twitches continue to drive activity in M1 through P24

Prior work at earlier ages demonstrated that twitch-related activity in sensorimotor cortex is quite dynamic across early development (Dooley and Blumberg, 2018; Dooley et al., 2021). Whereas limited evidence in adult rodents suggests that REM sleep twitches may drive activity in thalamus (Boscher et al., 2024) and M1 (Eckert et al., 2020), the apparent reduction in the proportion of twitch-responsive neurons in infant sensorimotor cortex (Dooley and Blumberg, 2018; Domínguez et al., 2021; Glanz et al., 2021) has led to the suggestion that the twitch-responsiveness seen in early infancy may be developmentally transient. In line with this notion, our findings reveal that the proportion of twitch-responsive neurons in M1 does decrease from 74% of neurons at P12 to 24% of neurons at P24. This transition, in which M1 neurons shift from responding to twitches to predominantly responding to wake movements, may reflect an expanding range of preferred stimuli as the cortex matures. Indeed, a similar progression—from simple to more complex motor maps—has been documented previously, albeit in rats older than the present investigation (Singleton et al., 2021). Nonetheless, a meaningful portion of M1 neurons were still twitch-responsive through P24.

Critically, this persistence of twitch-related activity in M1 through P24 suggests that twitches can play an important role in refining cortical circuits. At this age, neural activity in M1 is critical to the development of cortical motor control (Chakrabarty and Martin, 2005; Williams and Martin, 2015). For the neurons that remain twitch-responsive, twitch-related reafference is an important part of overall neural activity, and thus shapes M1's circuitry in preparation for its motor functions. These findings keep open the possibility that twitch-generated feedback continues to shape cortical circuitry throughout the lifespan. Altogether, these results underscore the significance of sleep and twitches in facilitating the final stages of M1's developmental transition toward adult-like motor control.

Developmental transition towards motor control

Our dual-site recordings sharpen the contrast between an established motor center (RN) and the still-maturing M1. In P24 pups, RN spiking not only precedes twitches and wake movements (see **Figure 7**) but is tuned to the kinematics of individual wake behaviors. Many RN neurons fire preferentially for specific forelimb movements and scale their response with movement amplitude (see **Figures 8-9**). Activity in M1, by comparison, lags movement onset (**Figure 5**) and shows little to no selectivity for direction (**Figure 9D**).

Thus, whereas RN already shows the movement-specific coding expected of a structure that generates specific behaviors, M1 activity during wake remains dominated by broad responses, rather than motor commands.

This dissociation implies that the emergence of cortical motor control will be accompanied by a qualitative shift in M1 coding. As corticospinal projections strengthen after P24 and ICMS-evoked movements first appear around P25 (Young et al., 2012; Singleton et al., 2021), we would predict that M1 neurons will begin to display the same relationship between direction- and amplitude-tuning that we observed in RN at P24. In other words, the movement-specific responses that we found in RN should migrate cortically as M1 begins driving behavior. Such a transition would parallel the progressive refinement we already see in the timing of M1's twitch related activity.

As for when M1 is fully developed, M1's forelimb motor map appears "adult-like" at P60 (Young et al., 2012; Singleton et al., 2021). However, these motor map milestones are subject to debate regarding what exactly they represent functionally, as some evidence suggests that the formation and reorganization of motor maps lags behind changes of the underlying circuitry (Kleim et al., 2004; Peters et al., 2017). Accordingly, it is plausible that discrete, behaviorally meaningful motor outputs from M1 begin earlier than can be detected via ICMS, and that the progressive refinement we observe in twitch-related M1 activity serves as a key developmental step leading to cortical motor control.

Taken together, our findings support a dynamic, two-stage model. Before weaning, neurons in RN initiate limb movements that dictate their direction and amplitude, whereas neurons in M1 reflect predicted and actual sensory feedback. As postnatal development proceeds, we expect that M1 will progressively adopt more RN-like movement selectivity. This interplay between M1 and RN likely reflects both the gradual maturation of corticospinal projections and the essential role of early reafferent signals in sculpting motor circuitry (Martin, 2005). Indeed, the incremental "pre-movement" activity we observe in M1 at P20 and P24 may be the first glimpse of its ability to shape behavior. Continuous sensorimotor feedback from both twitches and wake movements likely fuels this process, ensuring that the cortex inherits a well-calibrated, kinematically precise control scheme from brainstem motor centers, rather than creating one de novo.

Figure Legends

Figure 1. Recording environment, behavioral state quantification, and M1 recording verification

(A) Left: An illustration of the Mobile HomeCage used to record behavioral and electrophysiological data from head-fixed rat pups across sleep and wake. Right: A schematic of the rat brain with the primary somatosensory cortex (S1) shaded in gray, highlighting the approximate recording location in M1 and the reference/ground in the contralateral occipital cortex.
(B) Mean percentage of time spent in NREM sleep (light purple), REM sleep (dark purple), quiet wake (light green), and active wake (dark green) at each age. Numbers in each bar indicate the mean percentage of total recording time for that state across all animals.
(C) Representative coronal section stained for cytochrome oxidase showing the DiI-labeled electrode track in M1. Borders of primary somatosensory cortex are shown in gray; the DiI-labeled track is visible in the forelimb region of M1.
(D) Representative flattened cortical section stained for cytochrome oxidase showing the DiI-labeled electrode track in M1. Conventions as in C.

Figure 2. Behavioral and electrophysiological data across wake, NREM sleep, and REM sleep

For each age (P12, P16, P20, P24), a 50-s segment of continuous data is shown for wake, NREM sleep, and REM sleep. **Top to bottom**: ROI-based movement analysis of the entire rat (as detected by pixel-based motion detection), scored movements (wake movements during wake, twitches during REM sleep), M1 LFP, single-unit activity in M1 (each row corresponds to a separate unit), and biceps and nuchal EMG signals. Rows of scored twitches are forelimb, hindlimb, whisker, and tail, from top to bottom. These representative examples demonstrate distinct patterns of behavioral, neural, and muscular activity at each developmental age.

Figure 3. Developmental changes in oscillatory power during NREM and REM sleep

Normalized power spectra (1–50 Hz) at each age (P12, P16, P20, P24) are plotted relative to quiet wake. **(Left)** NREM sleep (light purple) exhibits a pronounced delta peak at all ages. **(Right)** REM sleep (dark purple) demonstrates an emerging theta peak from P16 onward. For each panel, data for the focal age are highlighted in color, whereas spectra for the other three ages are shown in gray for comparison. These findings illustrate the marked developmental changes in delta and theta oscillations across sleep states.

Figure 4. Movement responsiveness in M1 neurons across development
(A) Stacked bar plots showing the percentage of M1 neurons at each age (P12, P16, P20, P24) that respond to self-generated movements (i.e., twitches during REM sleep or wake movements during wake).
(B) Of the movement-responsive neurons identified in (A), the percentage that respond to twitches (purple), wake movements (green), or both (gray) are shown in stacked bars for each age.
(C) Representative M1 neurons from each age (P12, P16, P20, P24), illustrating raster plots (top) and perievent histograms (bottom) triggered on twitch onset (purple) or wake movement onset (green). Each histogram depicts firing rate changes relative to baseline, demonstrating strong but developmentally evolving movement-related activity in M1.

Figure 5. Temporal refinement of twitch- and wake-related M1 activity with age
(A) Top: Heatmaps showing twitch-triggered responses of all twitch-responsive M1 neurons across P12, P16, P20, and P24. Each row corresponds to a single neuron, and color intensity indicates firing rate. Bottom: Mean (±SEM) perievent histograms of these neurons for each age.
(B) Same as (A), but for wake-triggered responses of M1 neurons.
(C) Violin plots of the peak response time (relative to twitch onset) for twitch-responsive M1 neurons by age. The black line represents the mean of the distribution. ‘a’ indicates a significant difference from the preceding age, whereas ‘b’ indicates a significant difference from two ages prior.
(D) Same as (C), but for the width at half-height of twitch-triggered responses.
(E) Same as (C), but for the proportion of twitch-related activity that precedes movement. Collectively C-E reveals progressive temporal sharpening of M1 responses to twitches over the course of development.

Figure 6. RN recordings and responsiveness to movement at P24
(A) Schematic of the rat brain illustrating the dual recording sites in M1 and RN in P24 rats.
(B) Cartoon representation of a coronal section through the midbrain, showing the RN (red oval) and a representative electrode track for RN recordings. The rectangle on the left indicates the region enlarged on the right, which depicts the Nissl-stained section with the electrode track (red) passing through RN.
(C) Scatter plot of baseline RN neuronal activity during REM sleep (x-axis) versus wake (y-axis). Most RN units exhibit higher firing rates in REM sleep than in wake, and this difference is significant (asterisk).

(D) Stacked bar plots showing the proportion of RN neurons responsive to forelimb movements. The subplots on the right illustrate the fraction of those responsive neurons that react to twitches (purple), wake movements (green), or both (gray). This parallels the format of Figures 4A and 4B for M1.
(E) Representative RN neuron with raster plots (top) and averaged perievent histograms (bottom) for twitch- (left, purple) and wake-movement-triggered (right, green) responses.
(F) Heatmaps of all twitch-responsive RN neurons (top) and mean (±SEM; bottom) triggered on twitch onset (left) and wake movement onset (right), akin to Figures 5A and 5B for M1.

Figure 7. Comparison of twitch- and wake-related activity between M1 and RN at P24
(A) Heatmap of twitch-related responses of all twitch-responsive M1 neurons recorded during dual M1–RN recordings (compare to Figure 6F for RN).
(B) Top: Averaged, normalized twitch-triggered firing rates of M1 (blue) and RN (red) neurons. The gray shaded region indicates median displacement from the twitch. Bottom: The difference in normalized firing rates (M1 minus RN) shows RN activity precedes M1 activity.
(C) Same as A, but for wake movements.
(D) Same as B, but for wake movements.
(E) Violin plots of peak twitch-related activity for twitch-responsive M1 (blue) and RN (red) neurons, showing that RN responses peak significantly earlier than those in M1. Asterisk signifies a significant difference between groups.
(F) Violin plots of the width at half-height for neurons that show twitch-related activity. Conventions as in E.
(G) Violin plots of the proportion of activity that precedes twitch onset for neurons that show twitch-related activity. Conventions as in E.

Figure 8. Activity related to wake movements is highly variable in RN
(A) Raster and perievent histogram for all wake movements of a representative RN neuron that responds to only a subset of wake movements.
(B) Location of the right and left forelimbs (black and grey, respectively) for all triggered wake movements.
(C) Violin plots of the coefficient of variation of neural responses to wake movements for all M1 and RN neurons. Wake movement activity in RN is more variable than M1.
(D) The raster plot shown in **A**, sorted by the number of spikes in the response window.
(E) Raster and perievent histogram for the preferred wake movements.

(F) Location of the right and left forelimbs (green and grey, respectively) for wake movements accompanied by a neural response.
(G) Same as in **E**, but for the wake movements that did not produce a neural response.
(H) Same as in **F**, but for the wake movements that did not produce a neural response.

Figure 9. RN neurons exhibit greater movement selectivity than M1 neurons
(A) Polar plot for a representative RN neuron showing spike counts as a function of wake-movement direction (12 bins). The inset traces one example movement: the right forelimb starts at the red circle and reaches a maximum displacement of 25.9 mm at 129° (red arrow); this movement is highlighted with a red dot here and in B. Direction accounts for 25.8 % of the neuron's response variance ($\eta^2 = 0.258$).
(B) The same neuron's firing versus movement amplitude; green line, linear fit ($r^2 = 0.347$).
(C) For twitches, neither movement angle (η^2) nor amplitude (r^2) explains much response variance in M1 (left) or RN (right); only two neurons in each region exceed the 0.1 threshold (dashed lines).
(D) For wake movements, a larger subset of M1 neurons shows amplitude selectivity (elevated r^2), whereas RN neurons more often exhibit combined angle- and amplitude-tuning (both η^2 and $r^2 > 0.1$). The red-outlined point marks the example neuron from **A**–**B**.

References

Boscher F, Jumel K, Dvořáková T, Gentet LJ, Urbain N (2024) Thalamocortical Dynamics during Rapid Eye Movement Sleep in the Mouse Somatosensory Pathway. J Neurosci 44 Available at: https://www.jneurosci.org/content/44/25/e0158242024 [Accessed January 3, 2025].

Chakrabarty S, Martin JH (2005) Motor but not sensory representation in motor cortex depends on postsynaptic activity during development and in maturity. J Neurophysiol 94:3192–3198.

Domínguez S, Ma L, Yu H, Pouchelon G, Mayer C, Spyropoulos GD, Cea C, Buzsáki G, Fishell G, Khodagholy D, Gelinas JN (2021) A transient postnatal quiescent period precedes emergence of mature cortical dynamics Nelson SB, Moore T, Nelson SB, Colonnese MT, eds. eLife 10:e69011.

Dooley JC, Blumberg MS (2018) Developmental “awakening” of primary motor cortex to the sensory consequences of movement. eLife 7.

Dooley JC, Glanz RM, Sokoloff G, Blumberg MS (2020) Self-Generated Whisker Movements Drive State-Dependent Sensory Input to Developing Barrel Cortex. Curr Biol 30:2404-2410.e4.

Dooley JC, Sokoloff G, Blumberg MS (2021) Movements during sleep reveal the developmental emergence of a cerebellar-dependent internal model in motor thalamus. Curr Biol.

Eckert MJ, McNaughton BL, Tatsuno M (2020) Neural ensemble reactivation in rapid eye movement and slow-wave sleep coordinate with muscle activity to promote rapid motor skill learning. Philosophical Transactions of the Royal Society B: Biological Sciences 375:20190655.

Glanz RM, Dooley JC, Sokoloff G, Blumberg MS (2021) Sensory Coding of Limb Kinematics in Motor Cortex across a Key Developmental Transition. J Neurosci 41:6905–6918.

Gómez LJ, Dooley JC, Sokoloff G, Blumberg MS (2021) Parallel and Serial Sensory Processing in Developing Primary Somatosensory and Motor Cortex. J Neurosci 41:3418–3431.

Halley AC, Baldwin MKL, Cooke DF, Englund M, Krubitzer L (2020) Distributed Motor Control of Limb Movements in Rat Motor and Somatosensory Cortex: The Sensorimotor Amalgam Revisited. Cerebral Cortex 30:6296–6312.

Inagaki HK, Chen S, Ridder MC, Sah P, Li N, Yang Z, Hasanbegovic H, Gao Z, Gerfen CR, Svoboda K (2022) A midbrain-thalamus-cortex circuit reorganizes cortical dynamics to initiate movement. Cell 185:1065-1081.e23.

Kawai R, Markman T, Poddar R, Ko R, Fantana AL, Dhawale AK, Kampff AR, Olveczky BP (2015) Motor cortex is required for learning but not for executing a motor skill. Neuron 86:800–812.

Khazipov R, Sirota A, Leinekugel X, Holmes GL, Ben-Ari Y, Buzsáki G (2004) Early motor activity drives spindle bursts in the developing somatosensory cortex. Nature 432:758–761.

Kleim JA, Hogg TM, VandenBerg PM, Cooper NR, Bruneau R, Remple M (2004) Cortical synaptogenesis and motor map reorganization occur during late, but not early, phase of motor skill learning. J Neurosci 24:628–633.

Küchler M, Fouad K, Weinmann O, Schwab ME, Raineteau O (2002) Red nucleus projections to distinct motor neuron pools in the rat spinal cord. Journal of Comparative Neurology 448:349–359.

Lopez-Virgen V, Macías M, Rodriguez-Moreno P, Olivares-Moreno R, de Lafuente V, Rojas-Piloni G (2023) Motor cortex projections to red and pontine nuclei have distinct roles during movement in the mouse. Neuroscience Letters 807:137280.

Martin JH (2005) The corticospinal system: From development to motor control. Neuroscientist 11:161–173.

Mathis A, Mamidanna P, Cury KM, Abe T, Murthy VN, Mathis MW, Bethge M (2018) DeepLabCut: markerless pose estimation of user-defined body parts with deep learning. Nat Neurosci 21:1281–1289.

Mukherjee D, Yonk AJ, Sokoloff G, Blumberg MS (2017) Wakefulness suppresses retinal wave-related neural activity in visual cortex. J Neurophysiol 118:1190–1197.

Murata Y, Colonnese MT (2018) Thalamus Controls Development and Expression of Arousal States in Visual Cortex. J Neurosci 38:8772–8786.

Pachitariu M, Steinmetz N, Kadir S, Carandini M, Kenneth D. H (2016) Kilosort: realtime spike-sorting for extracellular electrophysiology with hundreds of channels. bioRxiv:061481.

Peters AJ, Liu H, Komiyama T (2017) Learning in the rodent motor cortex. Annu Rev Neurosci 40:77–97.

Rho M-J, Lavoie S, Drew T (1999) Effects of Red Nucleus Microstimulation on the Locomotor Pattern and Timing in the Intact Cat: A Comparison With the Motor Cortex. Journal of Neurophysiology 81:2297–2315.

Rio-Bermudez CD, Sokoloff G, Blumberg MS (2015) Sensorimotor Processing in the Newborn Rat Red Nucleus during Active Sleep. J Neurosci 35:8322–8332.

Robert JE (1982) Development of Sleep Spindle Bursts During the First Year of Life. Sleep 5:39–46.

Rossant C, Harris KD (2013) Hardware-accelerated interactive data visualization for neuroscience in Python. Front Neuroinform 7:36.

Ruder L, Schina R, Kanodia H, Valencia-Garcia S, Pivetta C, Arber S (2021) A functional map for diverse forelimb actions within brainstem circuitry. Nature 590:445–450.

Sauerbrei BA, Guo JZ, Cohen JD, Mischiati M, Guo W, Kabra M, Verma N, Mensh B, Branson K, Hantman AW (2020) Cortical pattern generation during dexterous movement is input-driven. Nature 577:386–391.

Seelke AM, Blumberg MS (2008) The microstructure of active and quiet sleep as cortical delta activity emerges in infant rats. Sleep 31:691–699.

Seelke AM, Dooley JC, Krubitzer LA (2012) The emergence of somatotopic maps of the body in S1 in rats: the correspondence between functional and anatomical organization. PloS one 7.

Singleton AC, Brown AR, Teskey GC (2021) Development and plasticity of complex movement representations. J Neurophysiol 125:628–637.

Sokoloff G, Dooley JC, Glanz RM, Wen RY, Hickerson MM, Evans LG, Laughlin HM, Apfelbaum KS, Blumberg MS (2021) Twitches emerge postnatally during quiet sleep in human infants and are synchronized with sleep spindles. Current biology 31:3426–3432.

Szymusiak R, Satinoff E (1981) Maximal REM sleep time defines a narrower thermoneutral zone than does minimal metabolic rate. Physiology & Behavior 26:687–690.

Tiriac A, Blumberg MS (2016) Gating of reafference in the external cuneate nucleus during self-generated movements in wake but not sleep. eLife 5.

Tiriac A, Del Rio-Bermudez C, Blumberg MS (2014) Self-generated movements with “unexpected” sensory consequences. Curr Biol 24:2136–2141.

Ulfig N, Chan WY (2001) Differential expression of calcium-binding proteins in the red nucleus of the developing and adult human brain. Anat Embryol 203:95–108.

Williams PT, Martin JH (2015) Motor Cortex Activity Organizes the Developing Rubrospinal System. J Neurosci 35:13363–13374.

Williams PTJA, Kim S, Martin JH (2014) Postnatal maturation of the red nucleus motor map depends on rubrospinal connections with forelimb motor pools. J Neurosci 34:4432–4441.

Yang L, Martin JH (2023) Effects of motor cortex neuromodulation on the specificity of corticospinal tract spinal axon outgrowth and targeting in rats. Brain Stimulation Available at: https://www.sciencedirect.com/science/article/pii/S1935861X23017540 [Accessed April 26, 2023].

Yang W, Kanodia H, Arber S (2023) Structural and functional map for forelimb movement phases between cortex and medulla. Cell 186:162-177. e18.

Young NA, Vuong J, Teskey GC (2012) Development of motor maps in rats and their modulation by experience. J Neurophysiol 108:1309–1317.

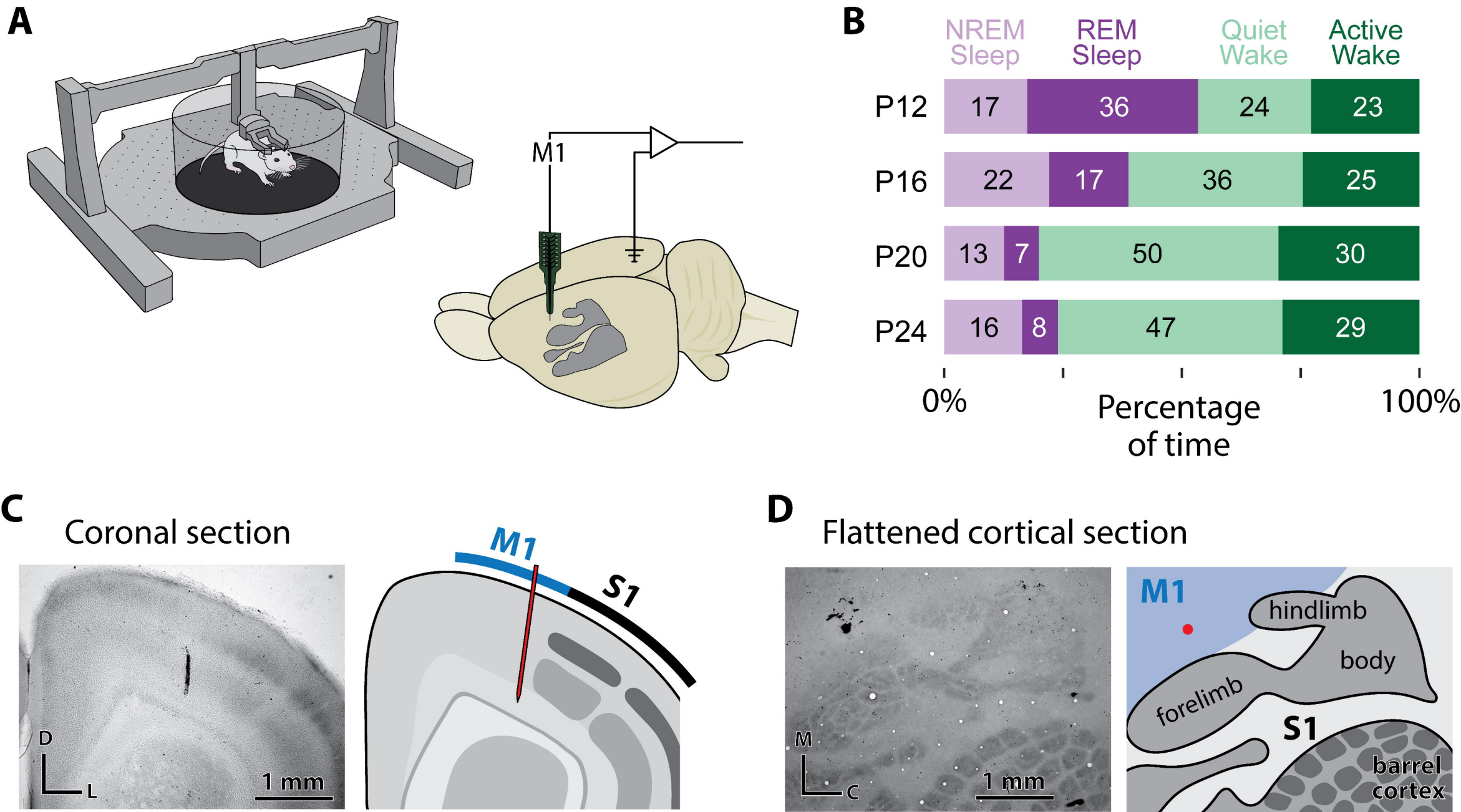
A
M1
B
NREM Sleep
REM Sleep
Quiet Wake
Active Wake
P12
17
36
24
23
P16
22
17
36
25
P20
13
7
50
30
P24
16
8
47
29
0%
Percentage of time
100%
C
Coronal section
M1
S1
D
L
1 mm
D
Flattened cortical section
M
C
1 mm
M1
hindlimb
body
forelimb
S1
barrel cortex

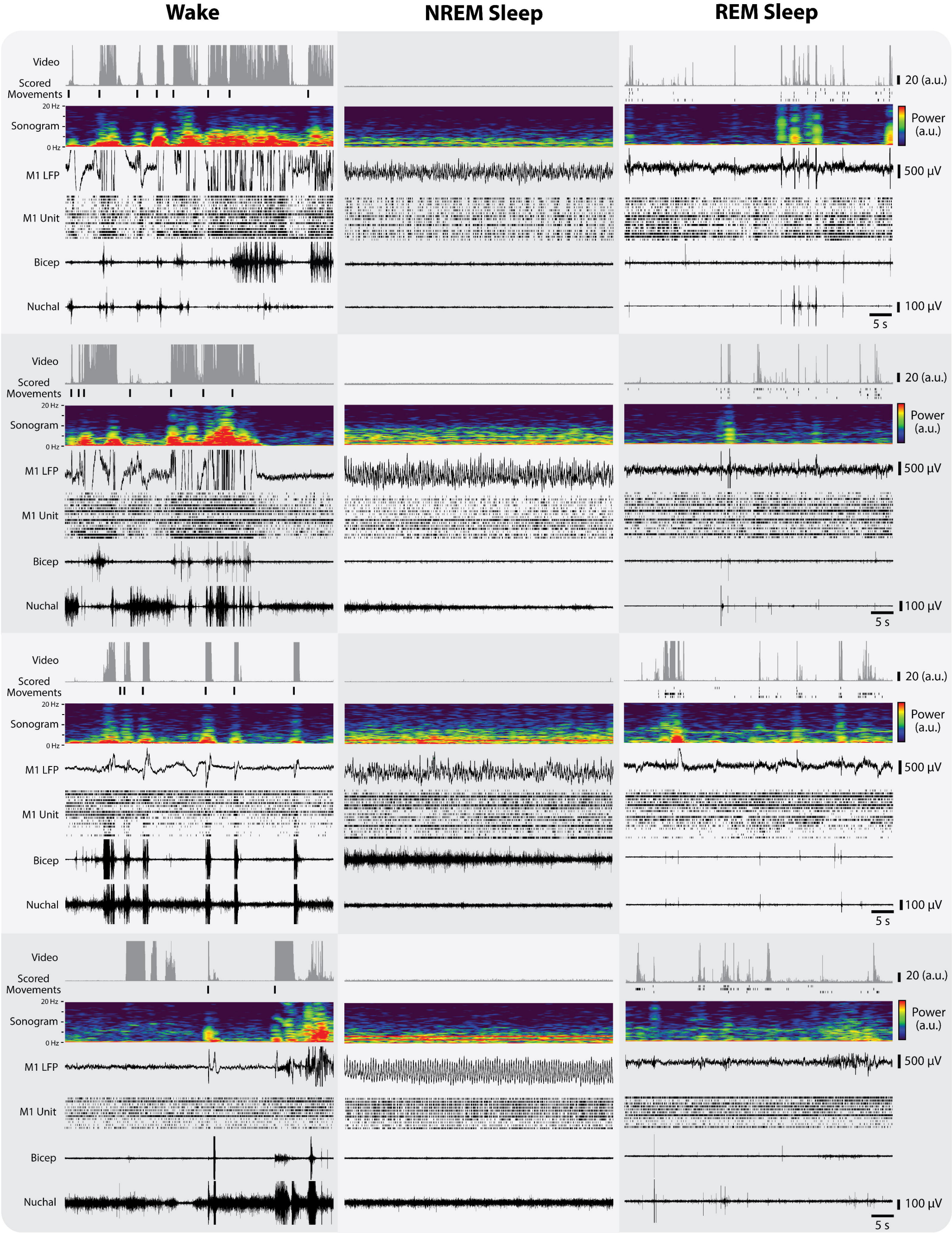
Wake
NREM Sleep
REM Sleep
P12
P16
P20
P24
Video
Scored Movements
Sonogram
20 Hz
0 Hz
M1 LFP
M1 Unit
Bicep
Nuchal
20 (a.u.)
Power (a.u.)
500 µV
100 µV
5 s

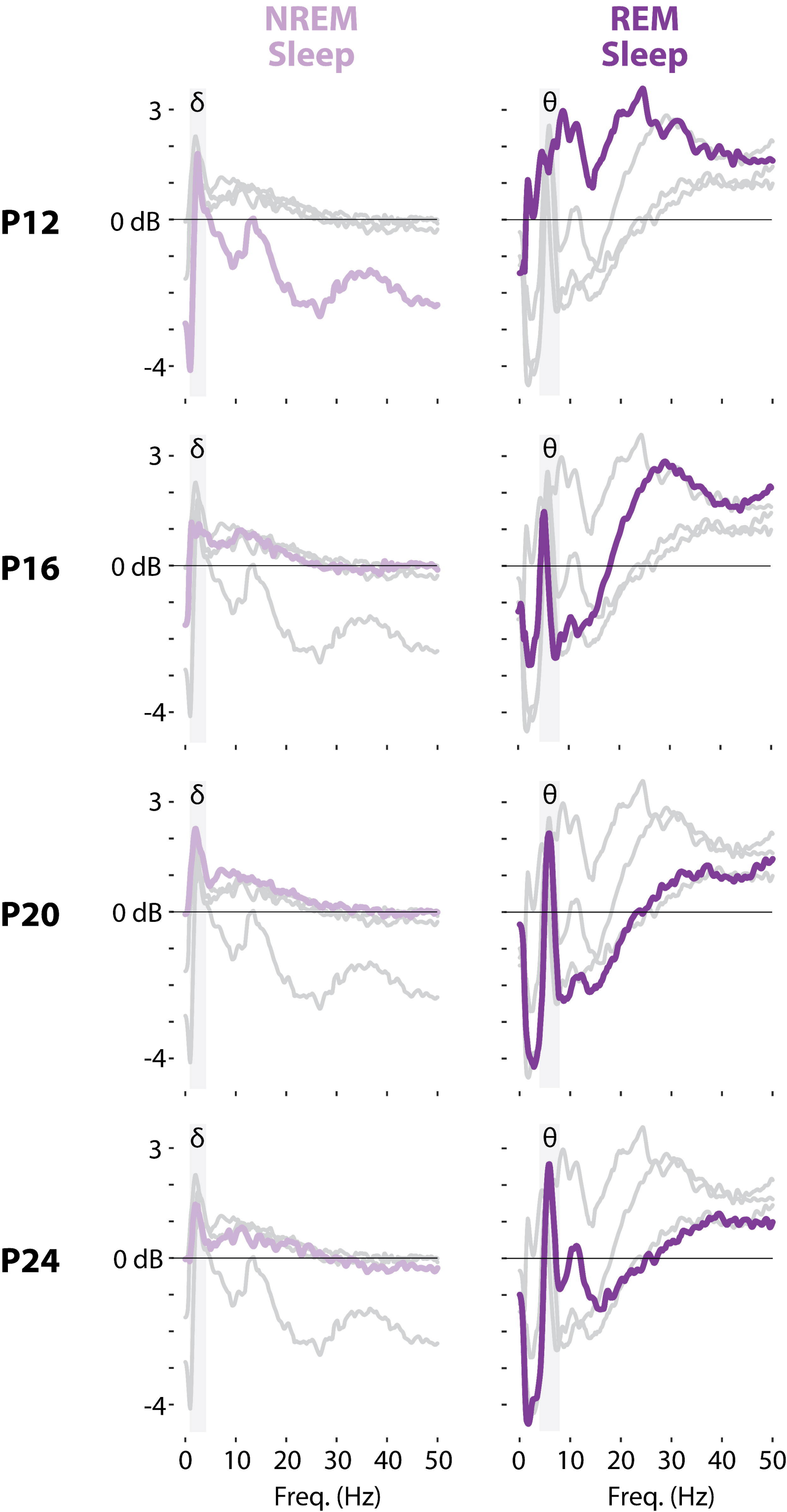
NREM Sleep
REM Sleep
P12
P16
P20
P24
δ
θ
3
0 dB
-4
0
10
20
30
40
50
Freq. (Hz)

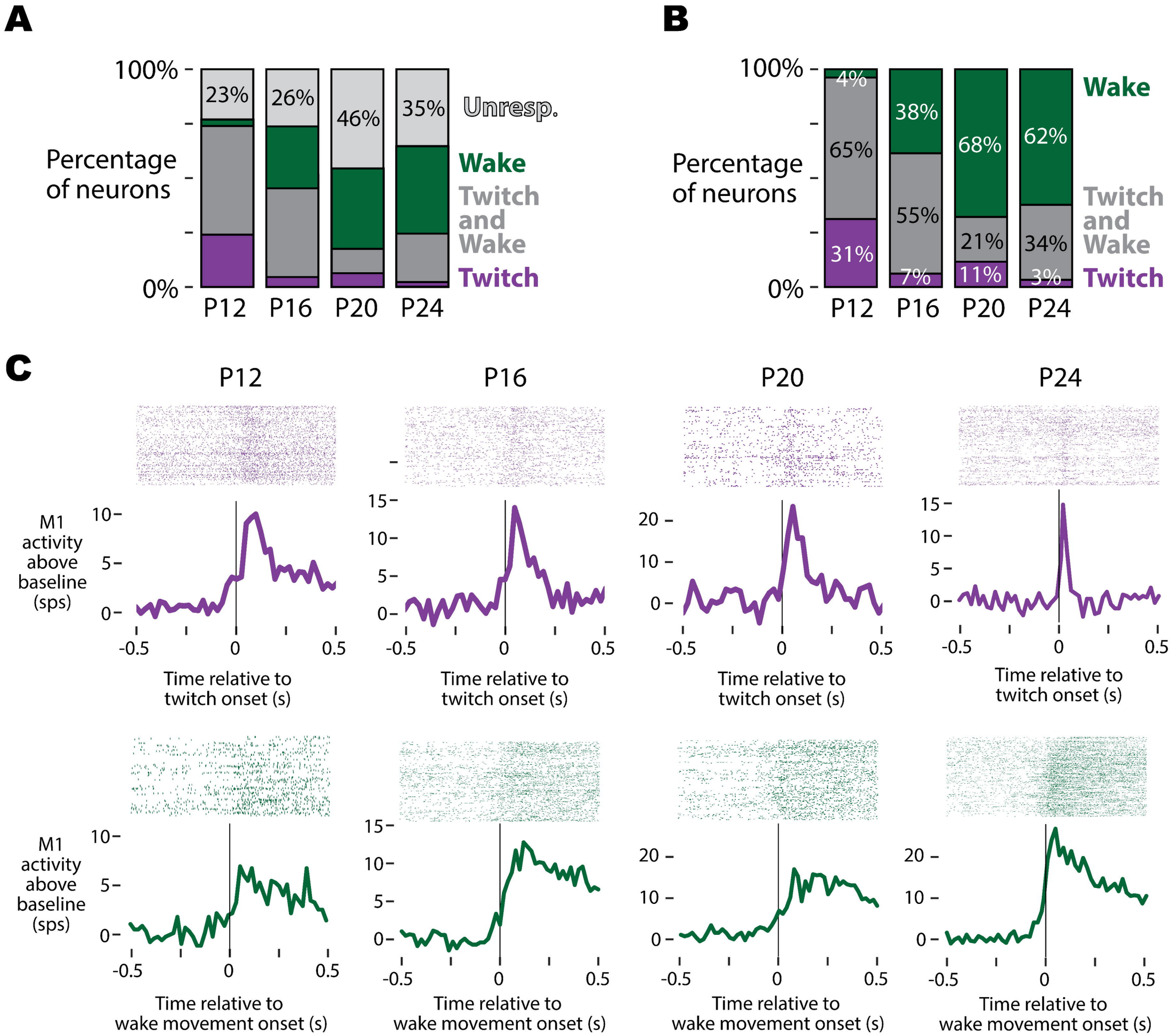
A
100%
0%
Percentage of neurons
23%
26%
46%
35%
P12
P16
P20
P24
Unresp.
Wake
Twitch and Wake
Twitch
B
100%
0%
Percentage of neurons
4%
65%
31%
38%
55%
7%
68%
21%
11%
62%
34%
3%
P12
P16
P20
P24
Wake
Twitch and Wake
Twitch
C
P12
P16
P20
P24
M1 activity above baseline (sps)
Time relative to twitch onset (s)
Time relative to wake movement onset (s)
-0.5
0
0.5

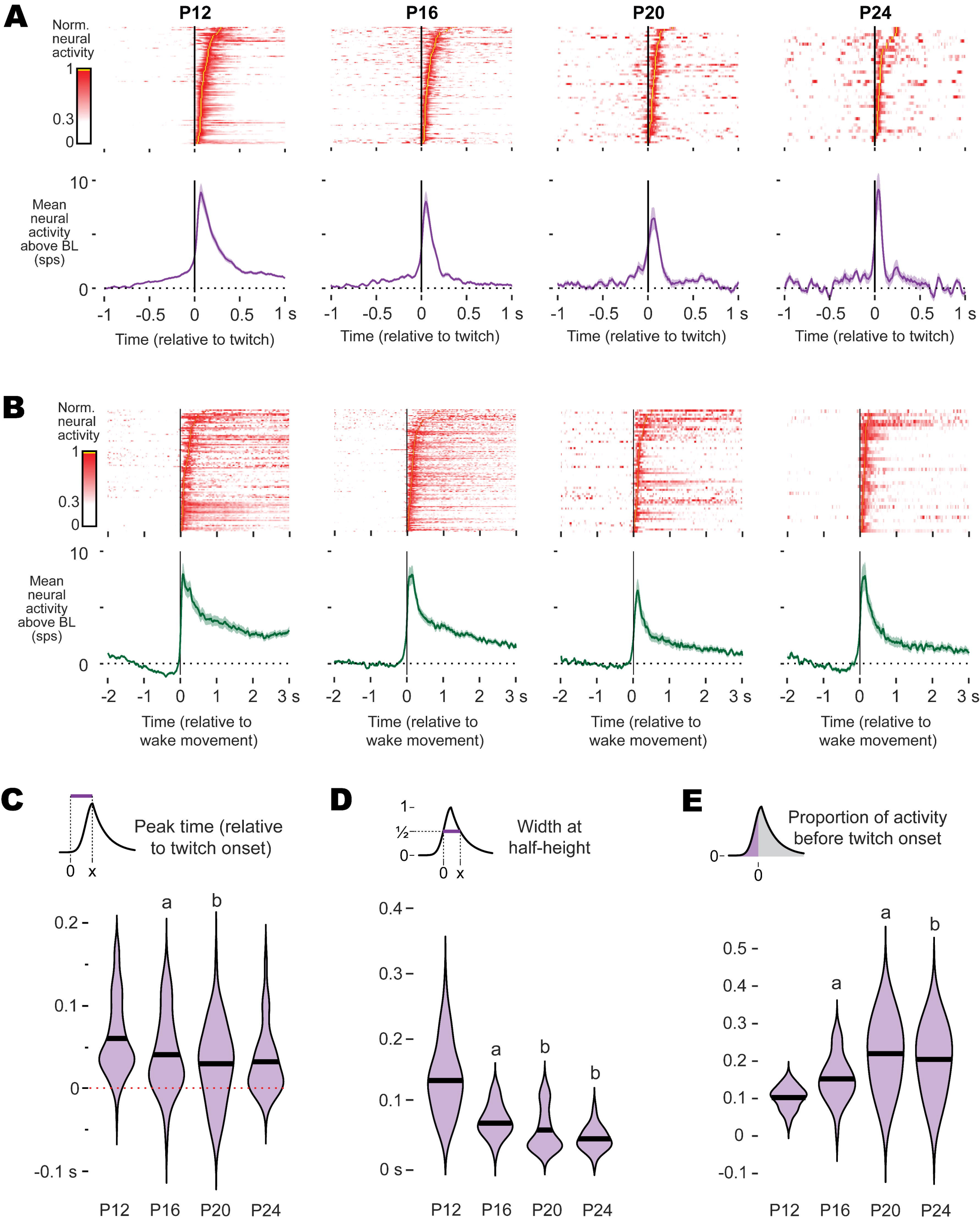
A
P12
P16
P20
P24
Norm. neural activity
1
0.3
0
Mean neural activity above BL (sps)
10
0
-1
-0.5
0
0.5
1 s
Time (relative to twitch)
B
Norm. neural activity
1
0.3
0
Mean neural activity above BL (sps)
10
0
-2
-1
0
1
2
3 s
Time (relative to wake movement)
C
Peak time (relative to twitch onset)
0
x
0.2
0.1
0
-0.1 s
a
b
P12
P16
P20
P24
D
1
½
0
Width at half-height
0.4
0.3
0.2
0.1
0 s
a
b
b
P12
P16
P20
P24
E
Proportion of activity before twitch onset
0
0.5
0.4
0.3
0.2
0.1
0
-0.1
a
a
b
P12
P16
P20
P24

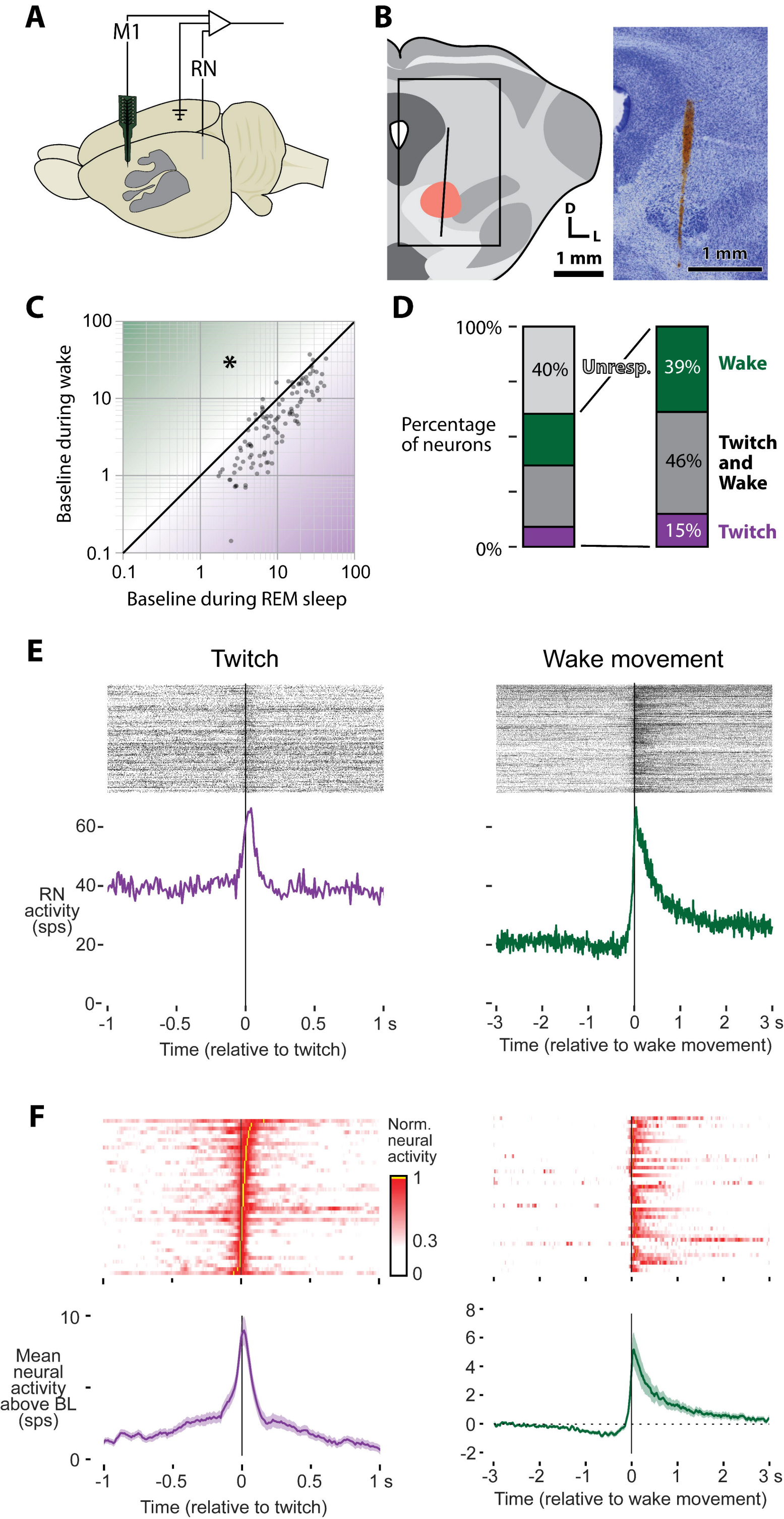
A
M1
RN
B
D
L
1 mm
1 mm
C
Baseline during wake
Baseline during REM sleep
100
10
1
0.1
0.1
1
10
100
*
D
100%
0%
Percentage of neurons
40%
Unresp.
39%
Wake
46%
Twitch and Wake
15%
Twitch
E
Twitch
Wake movement
RN activity (sps)
60
40
20
0
-1
-0.5
0
0.5
1 s
Time (relative to twitch)
-3
-2
-1
0
1
2
3 s
Time (relative to wake movement)
F
Norm. neural activity
1
0.3
0
Mean neural activity above BL (sps)
10
0
8
6
4
2
0
-2
-1
-0.5
0
0.5
1 s
Time (relative to twitch)
-3
-2
-1
0
1
2
3 s
Time (relative to wake movement)

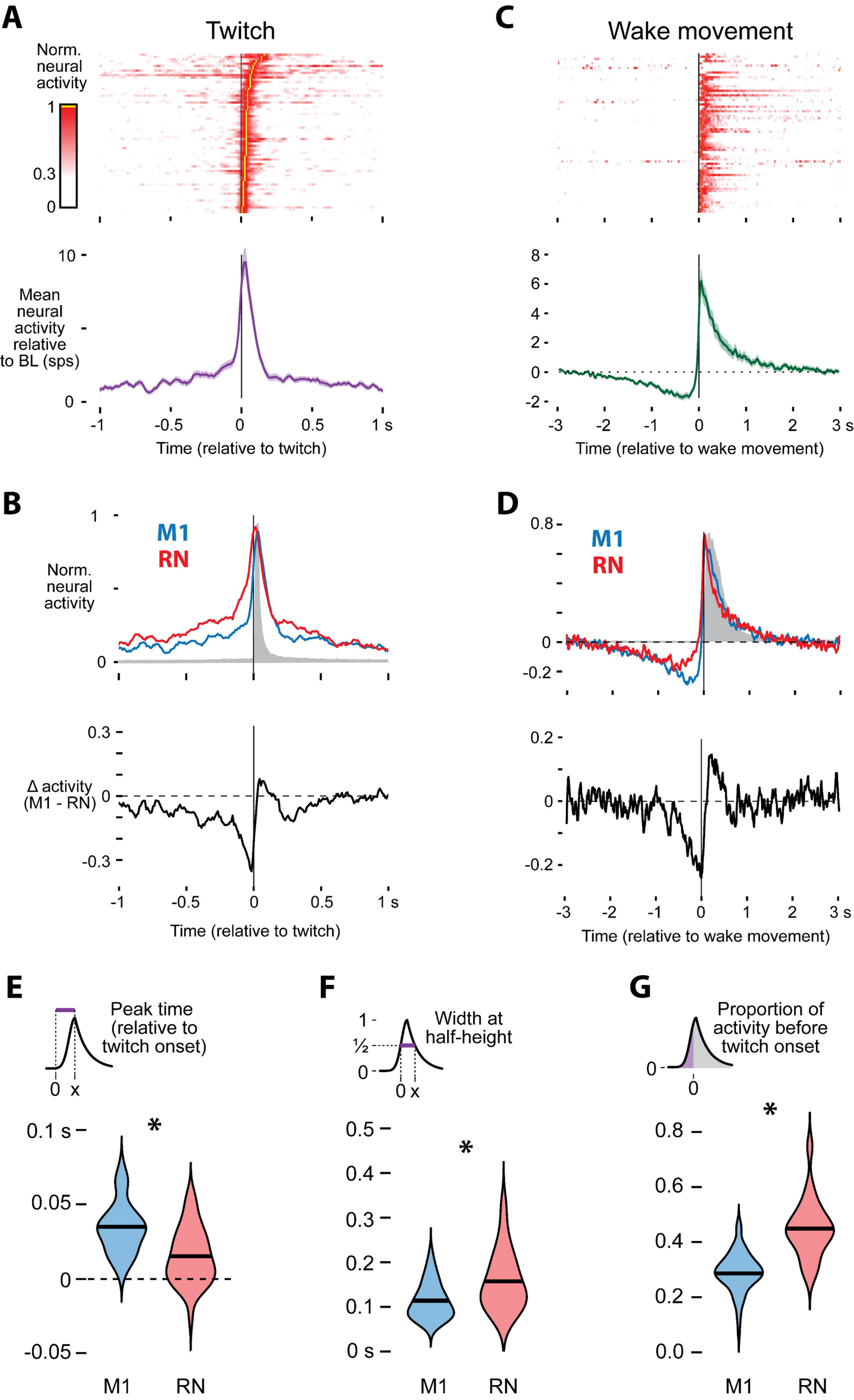
A
Twitch
Norm. neural activity
1
0.3
0
10
Mean neural activity relative to BL (sps)
0
-1
-0.5
0
0.5
1 s
Time (relative to twitch)
C
Wake movement
8
6
4
2
0
-2
-3
-2
-1
0
1
2
3 s
Time (relative to wake movement)
B
1
M1
RN
Norm. neural activity
0
0.3
Δ activity (M1 - RN)
0
-0.3
-1
-0.5
0
0.5
1 s
Time (relative to twitch)
D
0.8
M1
RN
0
-0.2
0.2
0
-0.2
-3
-2
-1
0
1
2
3 s
Time (relative to wake movement)
E
Peak time (relative to twitch onset)
0 x
0.1 s
0.05
0
-0.05
*
M1
RN
F
1
½
0
Width at half-height
0 x
0.5
0.4
0.3
0.2
0.1
0 s
*
M1
RN
G
Proportion of activity before twitch onset
0
0
0.8
0.6
0.4
0.2
0.0
*
M1
RN

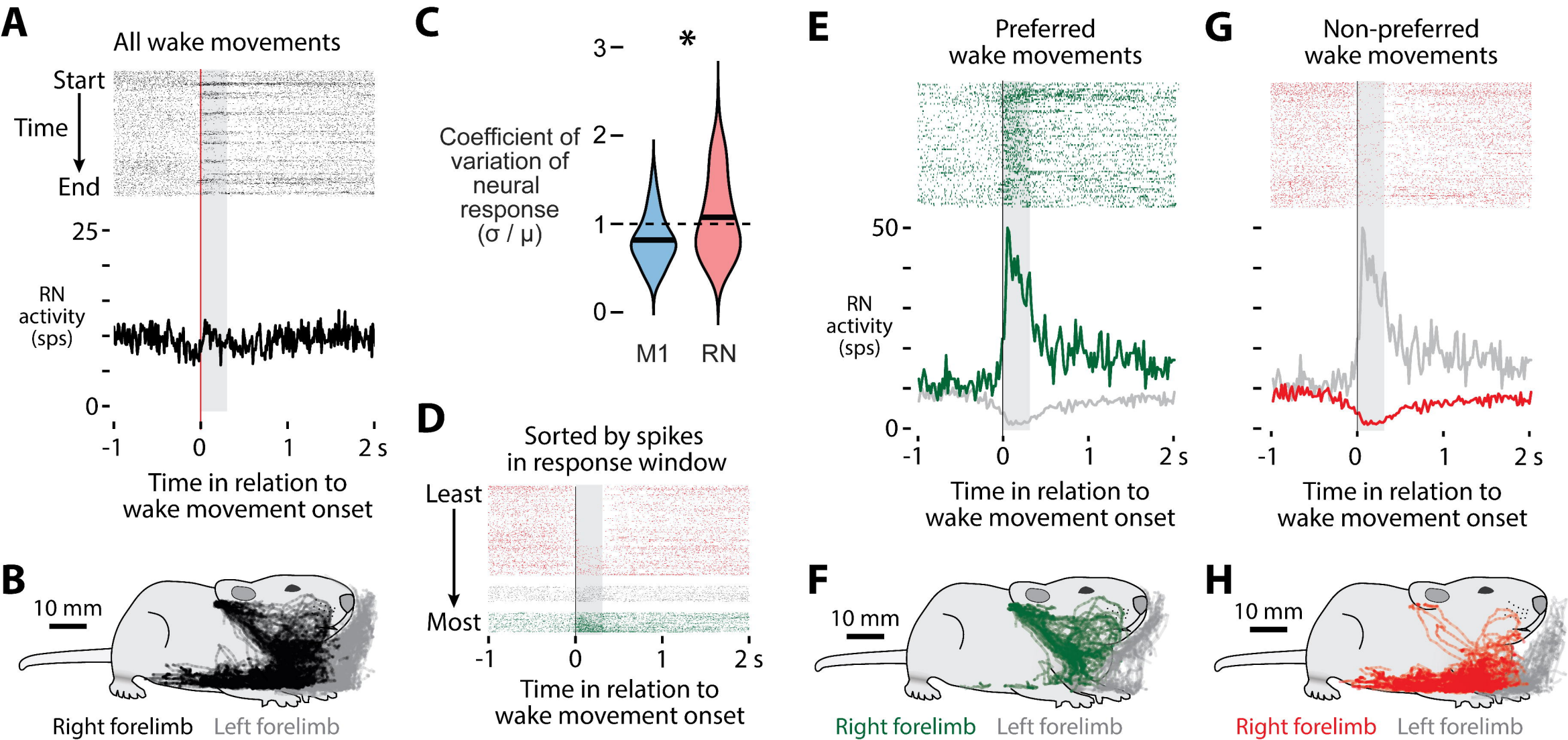
A
All wake movements
Start
Time
End
25
RN activity (sps)
0
-1
0
1
2 s
Time in relation to wake movement onset
B
10 mm
Right forelimb
Left forelimb
C
*
3
2
1
0
Coefficient of variation of neural response (σ / μ)
M1
RN
D
Sorted by spikes in response window
Least
Most
-1
0
1
2 s
Time in relation to wake movement onset
E
Preferred wake movements
50
RN activity (sps)
0
-1
0
1
2 s
Time in relation to wake movement onset
F
10 mm
Right forelimb
Left forelimb
G
Non-preferred wake movements
-1
0
1
2 s
Time in relation to wake movement onset
H
10 mm
Right forelimb
Left forelimb

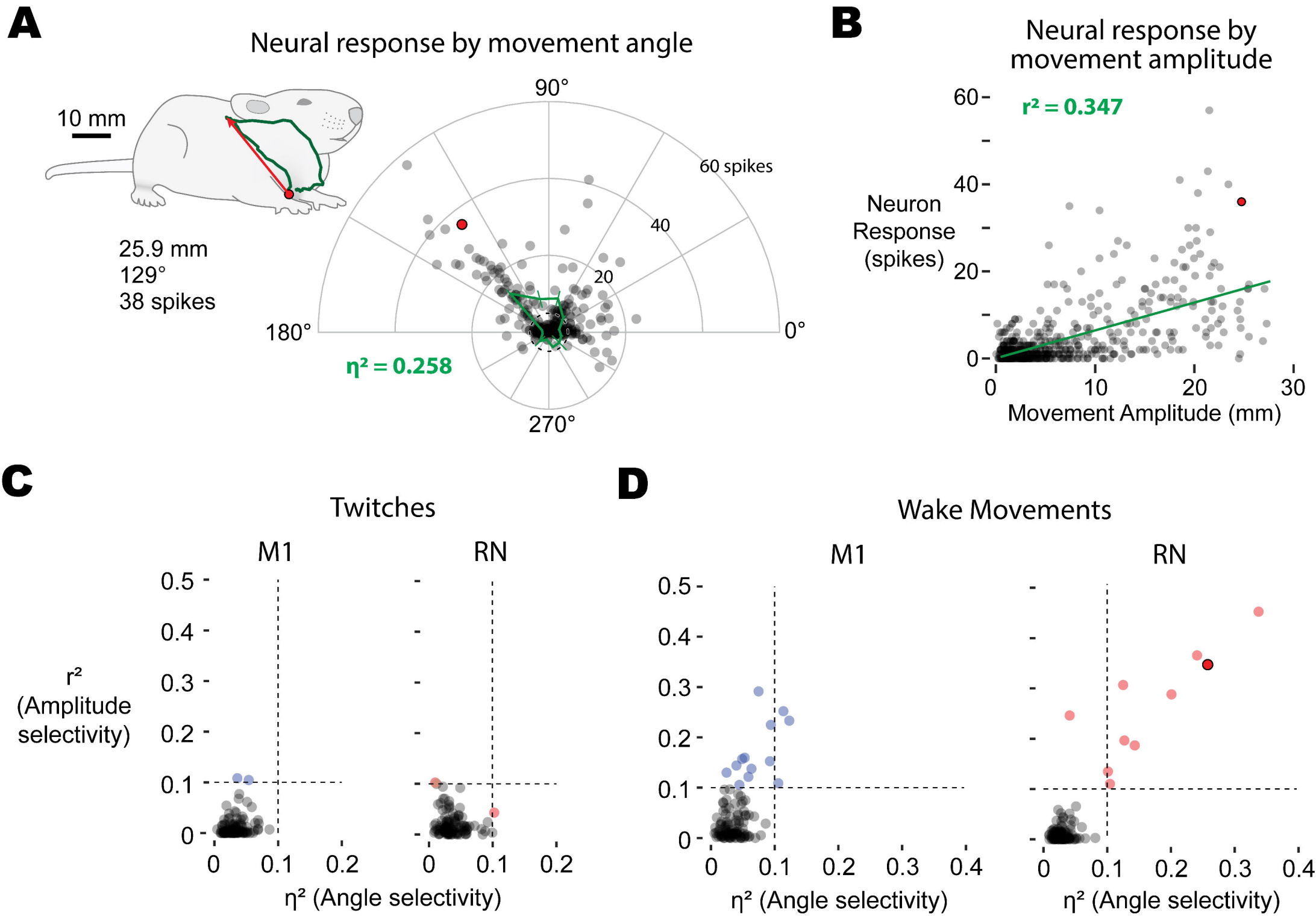
A
Neural response by movement angle
10 mm
25.9 mm
129°
38 spikes
90°
60 spikes
40
20
180°
0°
270°
η² = 0.258
B
Neural response by movement amplitude
r² = 0.347
Neuron Response (spikes)
60
40
20
0
0
10
20
30
Movement Amplitude (mm)
C
Twitches
M1
RN
r² (Amplitude selectivity)
0.5
0.4
0.3
0.2
0.1
0
0
0.1
0.2
η² (Angle selectivity)
D
Wake Movements
M1
RN
0.5
0.4
0.3
0.2
0.1
0
0
0.1
0.2
0.3
0.4
η² (Angle selectivity)